

Kerb and urban increment of highly time-resolved trace elements in PM₁₀, PM_{2.5} and PM_{1.0} winter aerosol in London during ClearfLo 2012

Article

Published Version

Creative Commons: Attribution 3.0 (CC-BY)

Open Access

Visser, S., Slowik, J. G., Furger, M., Zotter, P., Bukowiecki, N., Dressler, R., Flechsig, U., Appel, K., Green, D. C., Tremper, A. H., Young, D. E., Williams, P. I., Allan, J. D., Herndon, S. C., Williams, L. R., Mohr, C., Xu, L., Ng, N. L., Detournay, A., Barlow, J. F., Halios, C. H., Fleming, Z. L., Baltensperger, U. and Prévôt, A. S. H. (2015) Kerb and urban increment of highly time-resolved trace elements in PM₁₀, PM_{2.5} and PM_{1.0} winter aerosol in London during ClearfLo 2012. *Atmospheric Chemistry and Physics*, 15 (5). pp. 2367-2386. ISSN 1680-7316 doi: <https://doi.org/10.5194/acp-15-2367-2015> Available at <http://centaur.reading.ac.uk/55693/>

It is advisable to refer to the publisher's version if you intend to cite from the work.

Published version at: <http://dx.doi.org/10.5194/acp-15-2367-2015>

To link to this article DOI: <http://dx.doi.org/10.5194/acp-15-2367-2015>

Publisher: Copernicus Publications

All outputs in CentAUR are protected by Intellectual Property Rights law, including copyright law. Copyright and IPR is retained by the creators or other copyright holders. Terms and conditions for use of this material are defined in the [End User Agreement](#).

www.reading.ac.uk/centaur

CentAUR

Central Archive at the University of Reading

Reading's research outputs online



Kerb and urban increment of highly time-resolved trace elements in PM₁₀, PM_{2.5} and PM_{1.0} winter aerosol in London during ClearfLo 2012

S. Visser¹, J. G. Slowik¹, M. Furger¹, P. Zotter^{1,*}, N. Bukowiecki¹, R. Dressler², U. Flechsig³, K. Appel^{4,**}, D. C. Green⁵, A. H. Tremper⁵, D. E. Young^{6,***}, P. I. Williams^{6,7}, J. D. Allan^{6,7}, S. C. Herndon⁸, L. R. Williams⁸, C. Mohr^{9,****}, L. Xu¹⁰, N. L. Ng^{10,11}, A. Detournay¹², J. F. Barlow¹³, C. H. Halios¹³, Z. L. Fleming^{7,14}, U. Baltensperger¹, and A. S. H. Prévôt¹

¹Laboratory of Atmospheric Chemistry, Paul Scherrer Institute, Villigen, Switzerland

²Laboratory of Radiochemistry and Environmental Chemistry, Paul Scherrer Institute, Villigen, Switzerland

³Swiss Light Source, Paul Scherrer Institute, Villigen, Switzerland

⁴HASYLAB, DESY Photon Science, Hamburg, Germany

⁵School of Biomedical Sciences, King's College London, London, UK

⁶School of Earth, Atmospheric and Environmental Sciences, University of Manchester, Manchester, UK

⁷National Centre for Atmospheric Science, University of Manchester, Manchester, UK

⁸Aerodyne Research, Inc., Billerica, MA, USA

⁹Department of Atmospheric Sciences, University of Washington, Seattle, WA, USA

¹⁰School of Chemical and Biomolecular Engineering, Georgia Institute of Technology, Atlanta, GA, USA

¹¹School of Earth and Atmospheric Sciences, Georgia Institute of Technology, Atlanta, GA, USA

¹²Centre for Ecology and Hydrology, Penicuik, Midlothian, UK

¹³Department of Meteorology, University of Reading, Reading, UK

¹⁴Department of Chemistry, University of Leicester, Leicester, UK

* now at: Lucerne School of Engineering and Architecture, Bioenergy Research, Lucerne University of Applied Sciences and Arts, Horw, Switzerland

** now at: European XFEL, Hamburg, Germany

*** now at: Department of Environmental Toxicology, University of California, Davis, CA, USA

**** now at: Institute for Meteorology and Climate Research, Karlsruhe Institute of Technology, Karlsruhe, Germany

Correspondence to: M. Furger (markus.furger@psi.ch)

Received: 1 April 2014 – Published in Atmos. Chem. Phys. Discuss.: 17 June 2014

Revised: 8 February 2015 – Accepted: 9 February 2015 – Published: 4 March 2015

Abstract. Ambient concentrations of trace elements with 2 h time resolution were measured in PM_{10–2.5}, PM_{2.5–1.0} and PM_{1.0–0.3} size ranges at kerbside, urban background and rural sites in London during winter 2012. Samples were collected using rotating drum impactors (RDIs) and subsequently analysed with synchrotron radiation-induced X-ray fluorescence spectrometry (SR-XRF). Quantification of kerb and urban increments (defined as kerb-to-urban and urban-to-rural concentration ratios, respectively), and assessment of diurnal and weekly variability provided insight into sources

governing urban air quality and the effects of urban micro-environments on human exposure. Traffic-related elements yielded the highest kerb increments, with values in the range of 10.4 to 16.6 for SW winds (3.3–6.9 for NE) observed for elements influenced by brake wear (e.g. Cu, Sb, Ba) and 5.7 to 8.2 for SW (2.6–3.0 for NE) for other traffic-related processes (e.g. Cr, Fe, Zn). Kerb increments for these elements were highest in the PM_{10–2.5} mass fraction, roughly twice that of the PM_{1.0–0.3} fraction. These elements also showed the highest urban increments (~3.0), although no differ-

ence was observed between brake wear and other traffic-related elements. All elements influenced by traffic exhibited higher concentrations during morning and evening rush hours, and on weekdays compared to weekends, with the strongest trends observed at the kerbside site, and additionally enhanced by winds coming directly from the road, consistent with street canyon effects. Elements related to mineral dust (e.g. Al, Si, Ca, Sr) showed significant influences from traffic-induced resuspension, as evidenced by moderate kerb (3.4–5.4 for SW, 1.7–2.3 for NE) and urban (~ 2) increments and increased concentrations during peak traffic flow. Elements related to regional transport showed no significant enhancement at kerb or urban sites, with the exception of $\text{PM}_{10-2.5}$ sea salt (factor of up to 2), which may be influenced by traffic-induced resuspension of sea and/or road salt. Heavy-duty vehicles appeared to have a larger effect than passenger vehicles on the concentrations of all elements influenced by resuspension (including sea salt) and wearing processes. Trace element concentrations in London were influenced by both local and regional sources, with coarse and intermediate fractions dominated by traffic-induced resuspension and wearing processes and fine particles influenced by regional transport.

1 Introduction

Ambient particulate matter (PM) has long been recognized to have a detrimental effect on public health in urban areas (e.g. Dockery and Pope, 1994). Of particular interest are particles with an aerodynamic diameter less than $10\ \mu\text{m}$ (PM_{10}) as these particles can penetrate deeply into the lungs (Franklin et al., 2008; Zhou et al., 2011). Reche et al. (2012) reported even higher toxicity to human cells for the $\text{PM}_{2.5-1.0}$ than for the $\text{PM}_{10-2.5}$ fraction. Particle toxicity is known to vary significantly with PM composition and emission sources (Kelly and Fussell, 2012), with identified toxic constituents including soluble secondary inorganic particles, elemental and organic carbon, and especially metals. Effective mitigation strategies therefore require detailed, size-dependent characterization of particle composition and emission sources.

In addition to their direct effects on human health, metals and trace elements are of importance because their high source specificity and atmospheric stability make them effective tracers for source apportionment. In Europe, four main source types in PM_{10} are commonly identified: vehicles (with tracers including e.g. Fe, Ba, Zn, Cu), crustal materials (e.g. Al, Si, Ca, Fe), sea salt (mainly Na, Cl, Mg) and mixed industrial/fuel-oil combustion (mainly V, Ni, S) and secondary aerosol (mainly S) (Putaud et al., 2010; Viana et al., 2008). The contribution of mineral dust and sea salt in most urban areas is larger in PM_{10} than in $\text{PM}_{2.5}$ (Harrison et al., 2001; Weijers et al., 2011). Emissions from vehicle exhaust, industry and secondary aerosol are predominantly

emitted and formed as $\text{PM}_{1.0}$ or in $\text{PM}_{2.5}$ (Bukowiecki et al., 2010; Harrison et al., 2011; Richard et al., 2011). Several of these sources have been directly linked to adverse health effects. For example, the largest aerosol source of human toxicity in Barcelona was attributed to traffic activities (encompassing vehicle emissions, road dust and secondary nitrate), with fuel oil combustion and industrial emissions also contributing to increased cancer risk (Reche et al., 2012). Turoczci et al. (2012) observed higher toxicity from direct emissions (e.g. from traffic) than from photochemically processed aerosol.

The Clean Air for London project (ClearLo; www.clearflo.ac.uk) is a multinational effort to elucidate the processes driving poor air quality in London, implemented through comprehensive measurements of particle- and gas-phase composition, and meteorological parameters (Bohnenstengel et al., 2014). ClearLo builds upon recent modelling and monitoring studies in London (Arnold et al., 2004; Bohnenstengel et al., 2011, 2013; Harrison et al., 2012a; Mavrogrianni et al., 2011). Despite improved air quality, PM_{10} concentrations are not decreasing, resulting in frequent exceedances of the daily PM_{10} limit (Harrison et al., 2008). Such exceedances are caused by complex interactions of regional and local emission sources, together with meteorological factors such as wind speed, air mass origin and daily cycles of the atmospheric boundary layer (Charron and Harrison, 2005; Harrison and Jones, 2005; Jones et al., 2010). Currently, emissions by industrial sources and stationary combustion are modest, while traffic is thought to contribute up to 80 % of the total PM_{10} in London, compared to less than 20 % for the entire UK, according to emission inventories between 1970 and 2001 (Dore et al., 2003).

The spatial density of emission sources found in typical urban environments leads to elevated particle concentrations compared to nearby rural locations. As an example, buildings may influence local meteorology by restricting air circulation (street canyon effect), producing human exposures that are orders of magnitude higher than those predicted by regional dispersion models (Zhou and Levy, 2008). This provides both acute exposure risk and increased long-term exposure for those passing through regularly, thereby producing a non-negligible impact on public health. To assess the impact of such micro-environments, we here investigate London trace element concentrations in terms of increments, defined as the concentration ratios between an environment of interest and a reference site (Charron et al., 2007; Lenschow et al., 2001).

Only a few studies have investigated trace elements through simultaneous measurements at multiple sites. Harrison et al. (2012b) reported increments of kerbside-to-urban background sites in London for non-size-segregated aerosol with a time resolution of 1 to 4 days. Theodosi et al. (2011) found that at urban and suburban sites in Athens and a regional site in Finokalia, Greece, crustal elements dominate coarse particles ($\text{PM}_{10-2.5}$), whereas anthropogenic sources

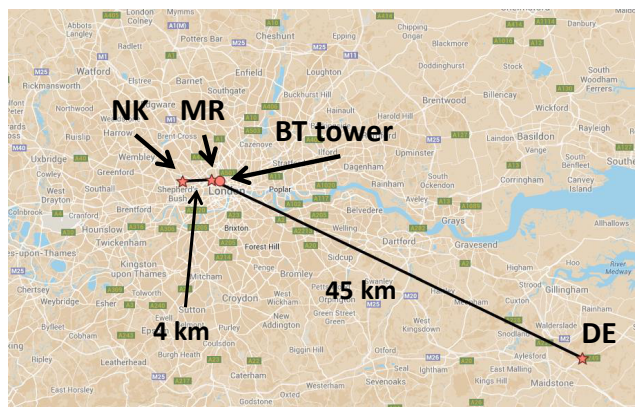


Figure 1. Map of southeastern UK. Indicated are the sampling sites MR (kerbside site Marylebone Road), NK (urban background site North Kensington), DE (rural site Detling), and the elevated BT Tower site for meteorological measurements (adapted from Google Maps).

such as fossil fuel combustion were confined to fine particles (V, Ni and Pb have > 70 % of their mass in $PM_{1.0}$). Bukowiecki et al. (2009a, 2010) examined trace elements in $PM_{10-2.5}$, $PM_{2.5-1.0}$ and $PM_{1.0-0.1}$ aerosol at street canyon and urban background sites in Zürich, Switzerland, and found increasing increments (note: 1 means no increment) with particle size from about 1.2 (fine mode) to 2.4 (coarse mode) (averaged over all elements). All these studies report increments close to 1 for elements originating from regional sources such as sea salt and Saharan dust, while local, especially traffic-related, sources yield increments around 2 for resuspension-related elements and between 3 and 5 for traffic-related elements. Additionally, the 1 h time resolution used by Bukowiecki et al. (2009a, 2010) enabled identification of enhanced increments for resuspension- and wearing-related elements like Si and Sb during peak traffic flows.

There is a need for more high time-resolved size-segregated increment analyses to assess the exposure to trace elements from emission sources within urban areas under varying meteorological conditions. Here we present size-segregated measurements of aerosol trace elements with 2 h time resolution performed simultaneously at kerbside and urban background sites in London, and a rural site outside London. We assess the effects of urban micro-environments on human exposure to particulate pollutants through the quantification of urban and kerb increments. These exposures are further investigated in terms of contributing emission sources, diurnal and weekly variability, local wind patterns and regional transport effects.

2 Methods

2.1 Measurement campaigns

The ClearfLo project was a measurement programme in and around London lasting 2 years (2011–2012) and including two month-long intensive observation periods (IOPs) in 2012 (Bohnenstengel et al., 2014). This paper focuses on the winter IOP lasting from 6 January to 11 February 2012. Measurements took place at three sampling sites located at or near permanent air quality measurement stations in the Automatic Urban and Rural Network (AURN): a kerbside site close to a very busy road, an urban background site in a residential area, and a rural background site away from direct emission sources (see Fig. 1).

The urban background sampling site was at the grounds of the Sion Manning Secondary School in North Kensington (NK, lat $51^{\circ}31'21''$ N, long $0^{\circ}12'49''$ W). NK is situated within a highly trafficked suburban area of London (Bigi and Harrison, 2010; Harrison et al., 2012a). During the ClearfLo IOPs this site served as the main measurement site and was upgraded with a full suite of particle- and gas-phase instruments, and instruments to measure meteorological parameters (Bohnenstengel et al., 2014). The kerbside site was located at Marylebone Road (MR, lat $51^{\circ}31'21''$ N, long $0^{\circ}09'17''$ W) about 4.1 km to the east of NK (Charron and Harrison, 2005; Harrison et al., 2011). This site is located at the southern side of a street canyon, with an axis running approximately 260 to 80° . Measurements took place at 1 m from a busy six-lane road with a traffic flow of approximately 73 000 vehicles per day of which 15 % consist of heavy-duty vehicles. Braking and stationary vehicle queues are frequent at the site due to a heavily used pedestrian light-controlled crossing (65 m west of MR) and a signal-controlled junction (200 m west of MR). The rural site at the Kent Showgrounds at Detling (DE, lat $51^{\circ}18'07''$ N, long $0^{\circ}35'22''$ E) was approximately 45 km to the southeast of London downtown on a plateau at 200 m a.s.l. surrounded by fields and villages, and was close to the permanent measurement station of Kent and Medway Air Quality Monitoring Network. The site provides excellent opportunities to compare the urban and kerbside air pollution with the rural background pollution levels (Bohnenstengel et al., 2014; Mohr et al., 2013). A busy road with ~ 160 000 vehicles per day is located approximately 150 m south of DE. Meteorological parameters were measured at DE and at the British Telecom (BT) Tower (lat $51^{\circ}31'17''$ N, long $0^{\circ}08'20''$ W), ~ 0.5 km east of MR (Harrison et al., 2012a).

Table 1. Measurement campaign details.

| Site | Start/end date | Site type | Sampling time | Inlet height | Sampling platform |
|------|--------------------|------------------|---------------|--------------|----------------------------|
| MR | 11 Jan–14 Feb 2012 | kerbside | 2 h | 4 m | container at 1 m from road |
| NK | 11 Jan–9 Feb 2012 | urban background | 2 h | 4 m | container |
| DE | 17 Jan–13 Feb 2012 | rural | 2 h | 1.5 m | grass field |

2.2 Instrumentation

2.2.1 RDI-SR-XRF

Rotating drum impactors

Rotating drum impactors (RDIs) were deployed at MR, NK and DE with a 2 h time resolution (see Table 1 for details). A detailed description of the RDI can be found in Bukowiecki et al. (2005, 2009c) and Richard et al. (2010). In short, aerosols are sampled through an inlet that removes all particles with aerodynamic diameter $d > 10 \mu\text{m}$ at a flow rate of $1 \text{ m}^3 \text{ h}^{-1}$. The particles are size segregated in three size ranges based on d – $\text{PM}_{10-2.5}$ (coarse), $\text{PM}_{2.5-1.0}$ (intermediate) and $\text{PM}_{1.0-0.3}$ (fine) – by passing sequentially through three rectangular nozzles of decreasing size. Particle deposition occurs via impaction on $6 \mu\text{m}$ thick polypropylene (PP) foils mounted on aluminium wheels and coated with Apiezon to minimize particle bouncing effects. After the last impaction stage a backup filter samples all remaining particles before the air passes through a pump. After each 2 h sampling interval the three wheels rotate stepwise to a blank section of the foil before a new sampling interval takes place. The small-size collection limit of the fine fraction was previously estimated at 100 nm (Bukowiecki et al., 2009c; Richard et al., 2010). However, new laboratory measurements of the RDI collection efficiency indicate an instrument-dependent (i.e. based on the machining of the specific nozzle) small-end cut point of approximately 290–410 nm (see Supplement A for details). This results in sampling of a smaller size range ($\text{PM}_{1.0-0.3}$) than the $\text{PM}_{1.0-0.1}$ range reported in previous studies, and influences the measured concentrations of elements with significant mass near this cut point (S, K and Pb).

SR-XRF analysis

Trace element analysis on the RDI samples was performed with synchrotron radiation-induced X-ray fluorescence spectrometry (SR-XRF) at the X05DA beamline (Flechsig et al., 2009) at the Swiss Light Source (SLS) at Paul Scherrer Institute (PSI), Villigen PSI, Switzerland and at Beamline L at Hamburger Synchrotronstrahlungslabor (HASYLAB) at Deutsches Elektronen-Synchrotron (DESY), Hamburg, Germany (beamline dismantled November 2012). The samples with the deposited particles were placed directly into the X-ray beam. Irradiation of the samples took place at a 45° angle for 30 s. The light spot of the incoming beam was ~ 140

by $70 \mu\text{m}$ at SLS (monochromatic excitation at 10.5 keV, in vacuum) and ~ 80 by $150 \mu\text{m}$ at HASYLAB (polychromatic excitation, in air). Fluorescence light produced by the elements in the samples was detected by energy-dispersive detectors (silicon drift detector at SLS, nitrogen cooled Si(Li)-detector at HASYLAB) at a 90° angle relative to the incoming beam. At SLS $K\alpha$ lines of the elements with atomic number $Z = 11-30$ (Na-Zn) were measured, and at HASYLAB $K\alpha$ lines of the elements with $Z = 22-56$ (Ti-Ba) and $L\alpha$ lines of $Z = 82$ (Pb).

The fluorescence counts per element were calibrated to the element mass concentration using multi-element standards, where each standard consisted of a set of preselected elements in five different concentrations ranging between 0.05 and $0.4 \mu\text{g cm}^{-2}$. The absolute element concentrations in these standards were determined with inductively coupled plasma-optical emission spectroscopy (ICP-OES). The absolute calibration factor for the SR-XRF system was referenced to Fe and determined from the linear relation between the SR-XRF response and the ICP-OES measurements. Because the fluorescence yield increases with atomic number Z , a relative calibration curve was constructed as follows: for each element present in the standards and having a detectable $K\alpha_1$ line, an absolute calibration factor was determined as for Fe, and a dimensionless relative response factor was calculated as the ratio of this absolute factor to that of Fe. These relative response factors were plotted as a function of line energy and a polynomial curve was fit to obtain response factors by interpolation for elements not present in the standard. In total 25 elements were quantified (Na, Mg, Al, Si, P, S, Cl, K, Ca, Ti, V, Cr, Mn, Fe, Ni, Cu, Zn, Br, Sr, Zr, Mo, Sn, Sb, Ba, Pb). Although some of these elements are not found in trace amounts in aerosols, for simplicity we refer here to trace elements for all analysed elements. Details of the methodology can be found elsewhere (Bukowiecki et al., 2005, 2008; Richard et al., 2010), with the following significant changes (see Supplement B for further details):

1. At SLS, we used an e2v SiriusSD detector (SiriusSD-30133LE-IS) and in-house built vacuum chamber to extend the measured range of elements down to Na and Mg.
2. Reference standards for calibration of element fluorescence counts to mass concentrations were produced on the same $6 \mu\text{m}$ PP substrate as used for RDI sampling allowing the use of identical geometry and irradiation

Table 2. Self-absorption correction factors.

| | Calibration standard 1 | | Calibration standard 2 | | PM _{10–2.5} sample | | PM _{2.5–1.0} sample | | Total correction factor ^d | | | |
|--|------------------------|-----------------------|------------------------|-----------------------|-----------------------------|-----------------------|------------------------------|-----------------------|--------------------------------------|-------------------|-------------------|-----------------------------|
| | AF ^c | <i>a</i> ^c | AF ^c | <i>a</i> ^c | AF ^c | <i>a</i> ^c | AF ^c | <i>a</i> ^c | | | | PM _{10–2.5} sample |
| Particle size (μm) ^a | 9.0 | | 9.0 | | 5.0 | | 1.6 | | | | | |
| Density (g cm ⁻³) ^b | 2.19 | | 2.27 | | 2.00 | | 2.00 | | | | | |
| Na | 0.22 | 0.49 | | | 0.43 | 0.40 | 0.74 | 0.40 | 0.52 | 0.30 | 0.22 | |
| Mg | | | 0.32 | 0.33 | 0.58 | 0.25 | 0.83 | 0.25 | 0.55 | 0.38 | 0.32 | |
| Al | 0.43 | 0.23 | | | 0.70 | 0.15 | 0.89 | 0.15 | 0.61 | 0.48 | 0.43 | |
| Si | | | 0.51 | 0.17 | 0.79 | 0.10 | 0.93 | 0.10 | 0.64 | 0.55 | 0.51 | |
| P | 0.60 | 0.13 | | | 0.85 | 0.07 | 0.95 | 0.07 | 0.70 | 0.63 | 0.60 | |
| S | | | 0.65 | 0.10 | 0.90 | 0.04 | 0.97 | 0.04 | 0.72 | 0.67 | 0.65 | |
| Cl | 0.71 | 0.08 | | | 0.88 | 0.05 | 0.96 | 0.05 | 0.80 | 0.73 | 0.71 | |
| K | | | 0.79 | 0.05 | 0.94 | 0.03 | 0.98 | 0.03 | 0.84 | 0.81 | 0.79 | |
| Ca | 0.82 | 0.05 | 0.76 | 0.06 | 0.95 | 0.02 | 0.98 | 0.02 | 0.87 ^e | 0.84 ^e | 0.82 ^e | |

^a Particle size given as geometric mean diameter.

^b Average density of the calibration standards and of ambient aerosol. The composition of calibration standard 1 is Na_{3.76}Al_{3.76}P_{3.76}Cl_{3.76}Ca_{3.76}CoN₈O₂₄, of calibration standard 2 Mg_{3.76}Si_{3.76}S_{3.76}K_{3.76}Ca_{3.76}CoN₇O₂₁, and of ambient samples C₃₉H₂₉N₁₀O₁₈S₃Fe.

^c Attenuation factors and *a* (μm⁻¹; $a = 2/3 \cdot \mu \cdot \rho$ with μ the mass attenuation coefficient (cm² g⁻¹) and ρ the particle mass density (g cm⁻³)) according to Eq. (4) in Formenti et al. (2010).

^d Total correction factor defined as ratios AF calibration standard / AF sample. Self-absorption effects are neglected in the PM_{1.0–0.3} samples; therefore these samples are only corrected for AF calibration standards.

^e Ca is corrected based on the average AF of calibration standards 1 and 2, and a calibration standard used to calibrate the elements Ti to Zn at SLS (Ca present in all three standards). Data for this third calibration standard are: particle size of 7.0 ± 2 μm, average density of 2.37 g cm⁻³ and AF and *a* for Ca of 0.89 and 0.03 μm⁻¹, respectively.

time for RDI samples and reference standards, thereby reducing uncertainties in absolute and relative calibrations.

- Data were processed with the Spectral Analysis for Multiple Instruments toolkit for XRF (SAMI-XRF) developed in-house within the IGOR Pro software environment (Wavemetrics, Inc., Portland, OR, USA). SAMI handles spectral fitting, quantification of associated uncertainties, and calculation and application of calibration parameters.

XRF is sensitive to self-attenuation of fluorescence radiation in the sample and depends on the sample composition and density, as well as particle layer thickness or particle size. The PM sample thickness of the coarse and intermediate fractions was maximally 0.7–1.5 μm at a maximum concentration of 10 μg m⁻³ total PM mass for each sample. For these fractions, self-absorption therefore mainly occurs within the individual particles (geometric mean of 5 and 1.6 μm for PM_{10–2.5} and PM_{2.5–1.0} fractions, respectively). For the fine fraction the PM layer is several micrometres thick, resulting in absorption inside the PM layer. However, this layer is mainly composed of species not resolved by SR-XRF (H, C, N, O). Furthermore, most mass of the lightest elements (Na–Ca) is restricted to the coarse and in-

termediate fractions (except for S and K). We therefore neglect self-absorption effects in the fine fraction samples. The calculated layer thickness of the dried calibration solution on the calibration standards is negligible at 3–60 nm, but the particle size of the dried droplets shows a geometric mean volume size distribution of 9 ± 5 μm and is therefore relevant for self-attenuation. Attenuation factors (AFs) were calculated for the calibration standards as well as for the coarse and intermediate fraction samples, as a function of density, mass attenuation coefficient and particle size, according to a simple attenuation model (Table 2; Formenti et al., 2010). For ambient samples and calibration standards, the attenuation length or penetration depth of X-rays for the heavier elements (i.e. above Ca) is greater than 33 μm, resulting in the near-complete excitation of these elements and correction factors below 3%. Self-absorption correction factors for Na–Ca are non-negligible, as discussed below and in Table 2. The attenuation of the calibration standards is taken into account for all samples, and additional corrections are applied to the coarse and intermediate samples. Calzolari et al. (2010) found comparable self-absorption effects for samples of different composition, total loading and sampling site. Because the elemental composition and particle size distribution of each sample are unknown, we assume a uniform correction for each element within a given size fraction. The overall

AF for Na to Ca are 0.52–0.87, 0.30–0.84 and 0.22–0.82 for coarse, intermediate and fine fraction samples, respectively.

2.2.2 Other measurements

Here a short description is given of relevant particle- and gas-phase instruments deployed at MR, NK and DE during the winter IOP. Daily PM₁₀ filter samples (midnight to midnight) were collected at MR and NK using Partisol 2025 samplers (Thermo Scientific, Inc.). The filters were digested in a 1 : 2 mixture of perchloric and hydrofluoric acid, and subsequently analysed by ICP-mass spectrometry (ICP-MS, calibration with NIST standards) for the determination of Na, Al, Ca, Ti, V, Mn, Fe, Ni, Cu, Zn, Sr, Mo, Sb, Ba and Pb. Additionally, Mg, K and Sn were available at NK. High-resolution time-of-flight aerosol mass spectrometers (HR-ToF-AMS, Aerodyne Research, Inc., Billerica, MA, USA) were deployed at MR (5 min time resolution), NK (5 min resolution every 30 min) and DE (2 min resolution) to characterize the non-refractory submicron aerosol components (DeCarlo et al., 2006). PM₁₀ mass concentrations were measured at all three sites with FDMS-TEOM (Filter Dynamics Measurement System Tapered Element Oscillating Microbalances; Thermo Scientific, Inc.) with a 1 h time resolution. NO_x measurements at MR and NK were performed with a NO_x chemiluminescent analyser with a single chamber and a single detector (API, A Series, model M200A; 15 min resolution). At DE, NO was determined with a Thermo Scientific 42i analyser and NO₂ with an Aerodyne CAPS-NO₂ (SN 1002) and an Aerodyne QCL-76-D. These NO and NO₂ measurements were summed together to obtain NO_x (1 min resolution). Equivalent black carbon (EBC) was measured with a two-wavelength Aethalometer ($\lambda = 370$ and 880 nm, model AE22, Magee Scientific) at MR and a seven-wavelength Aethalometer ($\lambda = 370$ –950 nm, model AE31, Magee Scientific) at NK and DE (5 min resolution), with a 2.5 μm cyclone at MR and DE and a 3.5 μm cyclone at NK. Traffic counts by vehicle group at MR from road sensors (number of vehicles per 15 min) were available as well. Wind direction and wind speed data for MR and NK were taken from the BT Tower (30 min resolution) where anemometers were placed to the top of an open lattice scaffolding tower of 18 m height on top of the main structure (190.8 m a.g.l.; Wood et al., 2010), whereas local data were used at DE (1 min resolution). Air mass origins were analysed with back trajectory simulations using the UK Met Office's Numerical Atmospheric Modelling Environment (NAME) dispersion model (Jones et al., 2007).

3 Data intercomparison and uncertainty

Here we compare RDI-SR-XRF data with independent filter data (24 h PM₁₀ trace element data analysed with ICP-MS; roughly 9 % uncertainty at a 95 % confidence interval) for 18 elements collected at MR and NK (no filter data were

available at DE). For this comparison, the three size ranges of the RDI were summed up to total PM₁₀ and averaged to the filter collection period. Details of the intercomparison results can be found in Supplement C. In short, the majority of the elements (Al, Ca, Ti, Mn, Fe, Cu, Zn, Sr, Sb, Ba) agree within approximately $\pm 50\%$ with Pearson's $R > 0.78$. Na and Mg agree as well, but have higher uncertainties due to self-absorption corrections. For the other elements, disagreement can be attributed to low or unknown filter sample extraction efficiencies (Ni, Mo) and differences in the particle size range sampled by the two measurement techniques (K, V, Sn, Pb). However, all elements are retained in the ensuing analysis as (1) they yield internally consistent results, as described in the following sections; (2) the ensuing analysis relies on relative changes/ratios per element across sites and is therefore not affected by a systematic bias in absolute magnitude.

The agreement between XRF and filter measurements in the present study compares favourably with that obtained in previous intercomparisons of trace element measurement techniques. Comparison of RDI-SR-XRF with daily element concentrations from a high-volume sampler followed by subsequent analysis using laboratory-based wavelength dispersive XRF (Bukowiecki et al., 2005) and by ICP-OES and ICP-MS (Richard et al., 2010) yielded slopes between 0.7 and 1.6 (except for S and K) with Pearson's $R > 0.5$. The spread/biases in these intercomparisons are not necessarily due to SR-XRF issues, as can be seen from a comparison by Salcedo et al. (2012) of ICP with proton-induced X-ray emission (PIXE) and AMS trace element measurements. Agreement between ICP and PIXE data was in the same range as between either method and the AMS data, with slopes ranging between 0.06 and 0.93 with Pearson's R from about 0.3 to 0.7.

Estimated uncertainties (per size fraction) and detection limits for each measured element are given in Supplement Table S3. A brief overview is presented here:

1. RDI sampling: the fluctuations in the flow rate are negligible within 5 % (Richard et al., 2010) and the uncertainties in the size cut-off are discussed in Supplement A.
2. SR-XRF accuracy: uncertainties in the absolute and relative calibrations affect absolute/fractional concentrations, but cancel out for relative changes/ratios, because all samples were measured under the same calibration conditions.
3. Issues such as imperfect flatness of the sample foils and detector dead-time corrections (Richard et al., 2010) reduce measurement precision but affect all elements with the same scaling factor.
4. SR-XRF measurement precision is affected by sample inhomogeneity, spectral analysis and self-absorption

correction uncertainties. Sample inhomogeneity was assessed by Bukowiecki et al. (2009c) and found to contribute $\pm 20\%$ uncertainty.

For most elements, except Mn and the lightest elements, sample inhomogeneity is the largest source of uncertainty. Mn is affected by spectral analysis uncertainties due to peak overlap with Fe, which is present in much higher concentrations. Therefore, a small bias in the energy calibration as function of detector channel leads to a large change in the peak area of Mn. Self-absorption effects are a significant source of uncertainty for the lightest elements (Na–Ca), but the good comparisons to the filter data suggest that the corrections lead to reasonable results. All data points lie well above their element detection limits, resulting in negligible uncertainties from the signal strength. In addition, RDI-SR-XRF measurements (both absolute/fractional and relative/ratio) are affected by atmospheric variability. This variability is likely the predominant source of the data spread evident in Table 3 and the following analyses.

4 Results and discussion

4.1 Trace element concentrations

During the ClearfLo winter IOP total mass concentrations of the analysed trace elements ranged from less than $0.1 \mu\text{g m}^{-3}$ to $\sim 10 \mu\text{g m}^{-3}$. Typically, concentrations were highest at MR and lower at NK and DE, and decreased with particle size. An overview of the obtained trace element concentrations as a function of size and site is given in Table 3. Note that S is not a trace element, but is commonly reported in trace element studies and is a good tracer for regional transport. Among the analysed trace elements, highest concentrations at MR were found for Na (28%), Cl (25%) and Fe (22%). At NK this was the case for Na (39%), Cl (29%) and Fe (11%) and at DE Na (40%), Cl (28%) and Fe (8%). Total analysed mass measured by the RDI-SR-XRF (trace elements +S) contributed on average 14% to the total PM_{10} mass (from FDMS-TEOM) of $32 (5\text{--}74) \mu\text{g m}^{-3}$ at MR (not extrapolated to the corresponding oxides), 10% to the mass of $23 (1.4\text{--}63) \mu\text{g m}^{-3}$ at NK and 7.4% to the mass of $17 (0.5\text{--}58) \mu\text{g m}^{-3}$ at DE.

A comparison between the contributions of coarse, intermediate and fine fractions to the total PM_{10} mass of each trace element is shown in Fig. 2 for the three sites. Trace elements at MR are dominated by the coarse fraction. Analysis in the following sections and previous measurements at this site (Charron and Harrison, 2005) suggest this is caused by large contributions of resuspension- and traffic-related mechanical abrasion processes, which primarily contribute to the coarse fraction. For all elements at this site, except S, Br and Pb, the coarse fraction contributes more than 50%. Mass fractions of intermediate mode elements to total PM_{10} are rather constant with contributions ranging from 11 to 27%. The fine fraction contributes up to 50% of total mass for S,

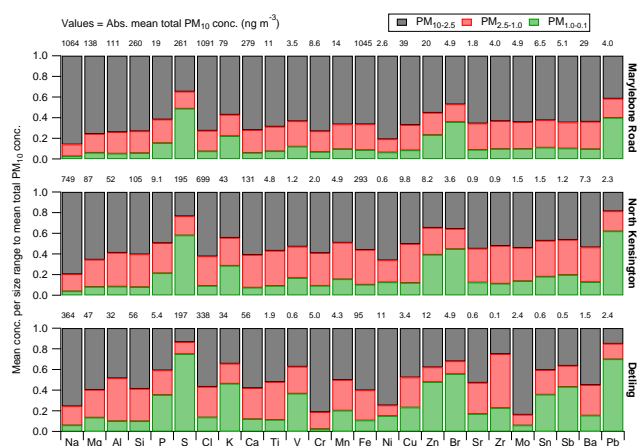


Figure 2. Relative contribution for trace elements in $\text{PM}_{10-2.5}$, $\text{PM}_{2.5-1.0}$ and $\text{PM}_{1.0-0.3}$ to total PM_{10} mean concentration per element at MR (top), NK (middle) and DE (bottom). Absolute mean total PM_{10} element concentrations are shown above each bar.

K, Zn, Br and Pb; for other elements fine contributions are less than 20%; S, K, Zn, Br and Pb are typically dominated by the fine fraction with known sources including heavy oil combustion (S, K, Zn; Lucarelli et al., 2000), traffic exhaust (Br, Pb; Formenti et al., 1996), industrial processes (Zn, Pb; Moffet et al., 2008), and secondary sulfate and wood combustion (S, K, Pb; Richard et al., 2011).

For most elements, particle mass contributions of the smaller size fractions are more important as one moves from kerbside to urban background to rural sites (Fig. 2). The relatively large fine fraction contribution at DE is probably caused by the absence of local traffic which results in lower contributions of resuspension- and traffic-related processes to total element concentrations. A different behaviour is observed for Cr, Ni and Mo with on average 80% of their mass at DE in the coarse fraction, compared to 73% at MR and 60% at NK. The time series of these coarse mode species are very spiky, are slightly enhanced with SW winds, but are not collocated with measurements of BC and AMS species, suggesting emissions from a local industrial source, potentially from stainless steel production (Querol et al., 2007; Witt et al., 2010) near DE rather than regional transport.

Comparing the contributions of groups of elements to total trace element concentrations at the sites provides an overview of local and regional sources affecting London; a detailed source apportionment study will be the subject of a future paper. Na, Mg and Cl are typical sea salt elements and contribute around 66% to the total PM_{10} trace element mass at all three sites, indicating that the air pollutant levels caused by elements are dominated by natural emission sources being transported to London. Mineral dust elements (Al, Si, Ca, Ti) mainly brought into the air via resuspension contribute on average 13% at MR, NK and DE. For some specific brake wear elements (Cu, Sb, Ba) these contributions

Table 3. Mean, median and 25–75th percentile trace element concentrations (ng m^{-3}) for $\text{PM}_{10-2.5}$, $\text{PM}_{2.5-1.0}$ and $\text{PM}_{1.0-0.3}$ at MR, NK and DE.

| Element | $\text{PM}_{10-2.5}$ | | | | $\text{PM}_{2.5-1.0}$ | | | | $\text{PM}_{1.0-0.3}$ | | | |
|------------------|----------------------|--------|-----------|-----------|-----------------------|--------|-----------|-----------|-----------------------|--------|-----------|-----------|
| | Mean | Median | 25th perc | 75th perc | Mean | Median | 25th perc | 75th perc | Mean | Median | 25th perc | 75th perc |
| Marylebone Road | | | | | | | | | | | | |
| Na | 913.7 | 854.2 | 447.9 | 1301.6 | 121.6 | 85.2 | 53.6 | 159.1 | 27.5 | 15.9 | 10.7 | 28.0 |
| Mg | 104.5 | 95.6 | 65.6 | 135.4 | 25.3 | 19.6 | 13.5 | 34.3 | 8.3 | 7.0 | 4.9 | 9.6 |
| Al | 82.4 | 66.5 | 44.9 | 102.7 | 23.1 | 20.7 | 15.4 | 28.3 | 5.8 | 5.4 | 3.6 | 7.2 |
| Si | 190.0 | 147.0 | 89.9 | 244.3 | 54.8 | 43.7 | 25.3 | 70.7 | 14.9 | 12.3 | 7.4 | 19.0 |
| P | 11.4 | 10.1 | 6.9 | 14.6 | 4.2 | 3.8 | 2.4 | 5.6 | 2.9 | 2.2 | 1.5 | 3.9 |
| S | 90.2 | 80.0 | 56.8 | 111.3 | 43.1 | 36.0 | 25.7 | 54.4 | 127.1 | 53.8 | 24.3 | 185.2 |
| Cl | 790.6 | 689.4 | 292.7 | 1164.4 | 217.4 | 110.0 | 30.6 | 329.1 | 81.2 | 25.2 | 5.1 | 103.4 |
| K | 36.2 | 32.4 | 23.1 | 44.0 | 13.1 | 11.3 | 7.6 | 17.4 | 14.1 | 9.4 | 6.3 | 18.4 |
| Ca | 201.9 | 152.4 | 93.6 | 265.6 | 62.0 | 43.9 | 26.7 | 79.3 | 16.7 | 12.3 | 7.4 | 20.7 |
| Ti | 7.5 | 5.9 | 3.4 | 10.0 | 2.6 | 2.0 | 1.2 | 3.6 | 0.8 | 0.7 | 0.4 | 1.1 |
| V | 2.2 | 1.9 | 1.1 | 2.9 | 0.9 | 0.8 | 0.4 | 1.1 | 0.4 | 0.4 | 0.2 | 0.6 |
| Cr | 6.3 | 3.6 | 2.0 | 6.0 | 1.7 | 1.4 | 0.9 | 2.4 | 0.6 | 0.4 | 0.3 | 0.7 |
| Mn | 9.4 | 7.7 | 4.6 | 12.2 | 3.4 | 2.9 | 2.0 | 4.4 | 1.4 | 1.0 | 0.6 | 1.7 |
| Fe | 693.1 | 601.7 | 347.0 | 929.9 | 259.9 | 226.8 | 136.4 | 348.6 | 90.4 | 75.8 | 43.6 | 122.3 |
| Ni | 2.1 | 0.6 | 0.4 | 1.0 | 0.3 | 0.2 | 0.1 | 0.4 | 0.2 | 0.1 | 0.1 | 0.2 |
| Cu | 26.0 | 22.9 | 12.6 | 33.3 | 9.5 | 8.2 | 4.6 | 12.5 | 3.3 | 2.6 | 1.4 | 4.5 |
| Zn | 10.9 | 8.9 | 5.2 | 14.1 | 4.3 | 3.6 | 2.0 | 5.6 | 4.6 | 3.0 | 1.6 | 6.5 |
| Br | 2.3 | 1.8 | 1.0 | 3.0 | 0.8 | 0.6 | 0.4 | 1.0 | 1.7 | 1.1 | 0.6 | 2.3 |
| Sr | 1.1 | 0.9 | 0.7 | 1.4 | 0.4 | 0.4 | 0.2 | 0.6 | 0.2 | 0.1 | 0.1 | 0.2 |
| Zr | 2.5 | 1.8 | 0.9 | 3.3 | 1.1 | 0.8 | 0.4 | 1.4 | 0.4 | 0.2 | 0.1 | 0.5 |
| Mo | 3.1 | 2.2 | 1.1 | 3.9 | 1.3 | 1.0 | 0.6 | 1.6 | 0.5 | 0.4 | 0.2 | 0.6 |
| Sn | 4.1 | 3.3 | 1.9 | 5.5 | 1.7 | 1.5 | 0.8 | 2.3 | 0.7 | 0.6 | 0.3 | 1.0 |
| Sb | 3.3 | 2.5 | 1.3 | 4.4 | 1.3 | 1.0 | 0.6 | 1.8 | 0.5 | 0.4 | 0.3 | 0.7 |
| Ba | 18.3 | 14.5 | 8.3 | 24.7 | 7.6 | 6.5 | 3.9 | 10.3 | 2.7 | 2.1 | 1.2 | 3.7 |
| Pb | 1.6 | 0.9 | 0.6 | 1.7 | 0.7 | 0.5 | 0.3 | 0.9 | 1.6 | 0.8 | 0.4 | 2.1 |
| North Kensington | | | | | | | | | | | | |
| Na | 595.1 | 511.6 | 269.6 | 897.9 | 123.5 | 87.1 | 56.4 | 163.7 | 28.6 | 14.2 | 9.8 | 31.7 |
| Mg | 57.2 | 49.9 | 30.2 | 83.9 | 23.0 | 17.9 | 12.7 | 30.8 | 7.1 | 5.2 | 3.1 | 8.8 |
| Al | 30.8 | 26.0 | 16.3 | 40.8 | 17.1 | 15.5 | 10.2 | 20.7 | 4.4 | 3.8 | 2.7 | 5.4 |
| Si | 63.1 | 51.2 | 25.6 | 78.7 | 33.1 | 26.5 | 14.7 | 45.0 | 8.3 | 5.9 | 3.5 | 10.2 |
| P | 4.5 | 4.0 | 2.3 | 6.3 | 2.7 | 2.3 | 1.4 | 3.3 | 1.9 | 1.4 | 0.8 | 2.4 |
| S | 45.8 | 40.7 | 27.5 | 61.7 | 36.1 | 28.8 | 20.3 | 44.2 | 113.3 | 53.1 | 24.6 | 137.0 |
| Cl | 435.6 | 343.1 | 110.6 | 702.3 | 199.2 | 79.1 | 18.2 | 289.8 | 63.7 | 9.9 | 2.5 | 66.6 |
| K | 18.9 | 16.7 | 10.8 | 25.9 | 11.5 | 9.9 | 6.7 | 16.1 | 12.2 | 8.1 | 4.9 | 14.8 |
| Ca | 79.9 | 60.7 | 35.0 | 99.0 | 41.7 | 31.1 | 17.5 | 50.1 | 9.7 | 7.1 | 4.0 | 11.6 |
| Ti | 2.7 | 1.7 | 0.9 | 3.2 | 1.6 | 1.2 | 0.5 | 2.3 | 0.4 | 0.3 | 0.1 | 0.5 |
| V | 0.6 | 0.4 | 0.2 | 0.7 | 0.4 | 0.3 | 0.1 | 0.5 | 0.2 | 0.2 | 0.1 | 0.3 |
| Cr | 1.2 | 0.8 | 0.4 | 1.5 | 0.6 | 0.5 | 0.3 | 0.8 | 0.2 | 0.1 | 0.04 | 0.2 |
| Mn | 2.4 | 1.7 | 1.0 | 3.0 | 1.7 | 1.5 | 0.8 | 2.2 | 0.8 | 0.5 | 0.1 | 0.9 |
| Fe | 163.8 | 120.8 | 69.9 | 202.6 | 98.8 | 72.7 | 39.0 | 126.0 | 30.1 | 18.5 | 9.6 | 34.8 |
| Ni | 0.4 | 0.2 | 0.1 | 0.4 | 0.1 | 0.1 | 0.04 | 0.2 | 0.1 | 0.1 | 0.02 | 0.1 |
| Cu | 4.9 | 3.6 | 1.8 | 6.4 | 3.7 | 2.5 | 1.4 | 4.6 | 1.2 | 0.6 | 0.4 | 1.4 |
| Zn | 2.9 | 1.9 | 1.0 | 3.4 | 2.1 | 1.5 | 0.8 | 2.8 | 3.2 | 1.9 | 0.8 | 4.3 |
| Br | 1.3 | 1.0 | 0.4 | 1.8 | 0.7 | 0.5 | 0.3 | 1.0 | 1.6 | 1.1 | 0.5 | 1.9 |
| Sr | 0.5 | 0.4 | 0.2 | 0.6 | 0.3 | 0.2 | 0.2 | 0.4 | 0.1 | 0.1 | 0.05 | 0.1 |
| Zr | 0.5 | 0.2 | 0.1 | 0.4 | 0.3 | 0.2 | 0.1 | 0.4 | 0.1 | 0.1 | 0.03 | 0.1 |
| Mo | 0.8 | 0.3 | 0.2 | 0.7 | 0.5 | 0.3 | 0.1 | 0.6 | 0.2 | 0.1 | 0.1 | 0.2 |
| Sn | 0.7 | 0.5 | 0.2 | 0.9 | 0.5 | 0.4 | 0.2 | 0.7 | 0.3 | 0.2 | 0.1 | 0.3 |
| Sb | 0.5 | 0.3 | 0.2 | 0.6 | 0.4 | 0.2 | 0.1 | 0.5 | 0.2 | 0.2 | 0.1 | 0.3 |
| Ba | 4.3 | 2.1 | 1.2 | 4.5 | 2.7 | 1.8 | 0.9 | 3.5 | 1.0 | 0.6 | 0.3 | 1.2 |
| Pb | 0.4 | 0.2 | 0.1 | 0.4 | 0.4 | 0.2 | 0.1 | 0.6 | 1.4 | 0.7 | 0.3 | 1.8 |

Table 3. Continued.

| Element | PM _{10–2.5} | | | | PM _{2.5–1.0} | | | | PM _{1.0–0.3} | | | |
|---------|----------------------|--------|-----------|-----------|-----------------------|--------|-----------|-----------|-----------------------|--------|-----------|-----------|
| | Mean | Median | 25th perc | 75th perc | Mean | Median | 25th perc | 75th perc | Mean | Median | 25th perc | 75th perc |
| Detling | | | | | | | | | | | | |
| Na | 271.9 | 194.7 | 17.2 | 437.0 | 66.2 | 37.2 | 13.0 | 82.2 | 21.3 | 11.4 | 5.0 | 28.3 |
| Mg | 27.5 | 20.8 | 5.2 | 39.9 | 12.4 | 8.8 | 2.7 | 17.1 | 6.2 | 4.4 | 1.6 | 7.7 |
| Al | 15.6 | 14.4 | 7.4 | 21.5 | 13.4 | 12.9 | 6.7 | 18.4 | 3.2 | 3.1 | 1.5 | 4.7 |
| Si | 32.5 | 26.3 | 13.8 | 41.5 | 17.3 | 13.7 | 6.1 | 25.3 | 5.5 | 4.3 | 2.4 | 7.9 |
| P | 2.2 | 1.8 | 0.8 | 2.9 | 1.3 | 1.0 | 0.5 | 1.7 | 1.9 | 1.0 | 0.5 | 2.4 |
| S | 26.1 | 22.8 | 4.9 | 34.6 | 22.3 | 20.4 | 8.8 | 32.1 | 145.2 | 38.8 | 18.0 | 157.4 |
| Cl | 189.6 | 40.5 | 2.9 | 303.7 | 99.1 | 6.8 | 1.9 | 109.0 | 45.4 | 7.3 | 2.4 | 40.4 |
| K | 11.7 | 10.0 | 2.9 | 14.9 | 6.6 | 6.1 | 2.1 | 10.1 | 15.7 | 6.4 | 2.9 | 15.6 |
| Ca | 32.5 | 24.9 | 9.6 | 40.3 | 16.7 | 12.3 | 4.9 | 21.0 | 6.7 | 4.1 | 2.2 | 6.8 |
| Ti | 1.0 | 0.6 | 0.3 | 1.3 | 0.7 | 0.4 | 0.2 | 1.0 | 0.2 | 0.2 | 0.1 | 0.3 |
| V | 0.2 | 0.1 | 0.1 | 0.2 | 0.1 | 0.1 | 0.1 | 0.2 | 0.2 | 0.1 | 0.04 | 0.3 |
| Cr | 4.0 | 0.9 | 0.3 | 2.9 | 0.8 | 0.3 | 0.2 | 0.6 | 0.1 | 0.1 | 0.02 | 0.2 |
| Mn | 1.8 | 0.6 | 0.3 | 1.3 | 1.1 | 1.2 | 0.3 | 1.6 | 0.7 | 0.3 | <0.04 | 0.7 |
| Fe | 55.2 | 36.8 | 19.9 | 66.2 | 26.8 | 21.5 | 11.5 | 37.7 | 9.8 | 7.8 | 4.3 | 13.3 |
| Ni | 4.3 | 0.7 | 0.2 | 2.6 | 0.6 | 0.1 | 0.1 | 0.3 | 0.9 | 0.1 | 0.02 | 0.5 |
| Cu | 1.4 | 0.8 | 0.4 | 1.8 | 0.9 | 0.7 | 0.4 | 1.1 | 0.7 | 0.3 | 0.1 | 0.5 |
| Zn | 3.4 | 0.9 | 0.4 | 1.8 | 1.3 | 0.7 | 0.3 | 1.7 | 4.3 | 1.6 | 0.6 | 5.7 |
| Br | 1.1 | 0.4 | 0.1 | 1.3 | 0.4 | 0.2 | 0.1 | 0.5 | 1.9 | 1.1 | 0.5 | 2.4 |
| Sr | 0.2 | 0.2 | 0.1 | 0.3 | 0.1 | 0.1 | 0.05 | 0.2 | 0.1 | 0.04 | <0.03 | 0.1 |
| Zr | 0.03 | <0.03 | <0.03 | 0.1 | 0.1 | 0.05 | <0.03 | 0.1 | 0.03 | <0.03 | <0.03 | 0.04 |
| Mo | 1.9 | 0.1 | 0.1 | 0.7 | 0.2 | 0.1 | 0.04 | 0.2 | 0.1 | 0.1 | 0.03 | 0.1 |
| Sn | 0.3 | 0.1 | <0.06 | 0.2 | 0.2 | 0.1 | 0.1 | 0.2 | 0.2 | 0.1 | 0.1 | 0.3 |
| Sb | 0.2 | 0.1 | <0.05 | 0.2 | 0.1 | 0.1 | <0.05 | 0.1 | 0.2 | 0.1 | <0.05 | 0.2 |
| Ba | 1.0 | 0.4 | 0.2 | 0.8 | 0.5 | 0.4 | 0.2 | 0.7 | 0.3 | 0.2 | <0.2 | 0.4 |
| Pb | 0.3 | 0.1 | <0.1 | 0.3 | 0.3 | 0.1 | 0.1 | 0.5 | 1.6 | 0.5 | 0.2 | 1.8 |

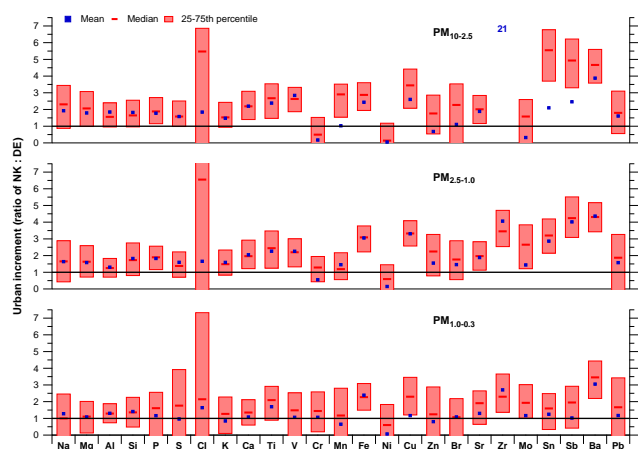


Figure 3. Mean, median and 25–75th percentile urban increment values for trace elements at NK relative to DE for PM_{10–2.5} (top), PM_{2.5–1.0} (middle) and PM_{1.0–0.3} (bottom). Note that the median of Zr in PM_{10–2.5} is below detection limit.

are 1.5, 0.6 and 0.4% at MR, NK and DE, respectively. Although these metals contribute a small fraction of total PM₁₀

mass concentrations, they induce adverse health effects. Xiao et al. (2013) e.g. found that Zn, Fe, Pb and Mn were the major elements responsible for plasmid DNA damage, whereas Kelly and Fussell (2012) found that increases in PM₁₀ as a result of increased Ni, V, Zn and Cu contributions showed highest mortality risks, as opposed to increased Al and Si.

4.2 Urban and kerb increment

4.2.1 Urban increment

The urban increment compares the trace element concentrations at the urban background site to the concentrations at the rural site, and is calculated here as the ratio of concentrations at NK to DE. Figure 3 shows the mean, median and 25–75th percentile urban increment ratios for the coarse, intermediate and fine fractions per element. Most elements, except Ni and coarse mode Cr, are enriched at the urban background site by factors between 1.0 and 6.5 (median ratios). Increments decrease towards smaller sizes. Ni and coarse mode Cr show higher concentrations at DE relative to NK, as does the mean value of coarse Mo. Especially at DE, Cr and Ni show strong correlations with Pearson's *R* of 0.85. As discussed in the

previous section, enhanced coarse mode Cr, Ni and Mo may indicate an industrial source near the rural site.

Coarse mode Zr exhibits low concentrations at DE, where the median value actually falls below detection limit, though discrete events above detection limit also exist. For this reason, the median-based urban increment is not plotted, while the mean ratio is driven by several large concentration peaks at NK, resulting in a large mean ratio of 21. In the case of Cl, a large spread in the urban increment values is seen for all three size ranges. Cl is likely depleted relative to other sea salt elements like Na and Mg (throughout the campaign Cl concentrations fall to 0, whereas Na and Mg concentrations remain positive) due to replacement by nitrate, and the extent of such depletion is greater in small particles (Nolte et al., 2008). At DE, Cl depletion seems apparent at all size ranges, whereas at MR depletion mainly takes place in the $PM_{1.0-0.3}$ fraction. NK shows Cl depletion especially in the $PM_{1.0-0.3}$ fraction, but to some extent also in intermediate mode particles.

For ease of discussion, we empirically group elements based on similar urban increment values. Mn, Fe, Cu, Zn, Zr, Mo, Sn, Sb and Ba show urban increments on average of 3.5 in the coarse, 3.1 in the intermediate and 2.0 in the fine fraction (Fig. 3). These have been identified as traffic-related elements by e.g. Amato et al. (2011), Bukowiecki et al. (2010), Minguillón et al. (2014), Richard et al. (2011) and Viana et al. (2008). Zr has also been linked to mineral dust (Moreno et al., 2013). We can understand that from analysing the enrichment factors (EFs) of these elements. EF is a measure of the enrichment of elements relative to the upper continental crust (UCC) and is defined as ppm metal in the sample divided by ppm metal in UCC with Si as reference material (UCC from Wedepohl, 1995). Zr is the only element in this traffic group that is depleted in the atmosphere relative to their UCC concentrations, but with concentrations at NK higher than at DE. Most other elements clearly indicate anthropogenic origin with $EF > 10$. Dependent on the method, Zr can be either grouped with traffic-related elements or with dust elements. The urban increments are similar to that of NO_x , where concentrations at NK were on average a factor of 4.9 higher than at DE (the mean concentration at NK was 68 ppb; at DE, 14 ppb). EBC, a marker for both traffic and wood burning emissions, had an urban increment of only 1.1 (concentration at NK 757 ng m^{-3} , at DE 633 ng m^{-3}), likely due to local wood burning emissions around DE (Mohr et al., 2013). Al, Si, Ca, Ti and Sr as markers for mineral dust (e.g. Amato et al., 2009; Lin et al., 2005; Lucarelli et al., 2000) show a factor 2.0 higher concentrations at NK relative to DE in the coarse, 1.9 in the intermediate and 1.6 in the fine fraction ($EF < 10$). These results indicate that moving from rural to urban backgrounds yields a larger relative increase in traffic than in mineral dust elements. Surprisingly, sea salt elements (Na, Mg, Cl) show higher concentrations at NK than at DE of up to a factor of 2 for the coarse mode, despite the expected dominance of regional over lo-

cal sources. This highlights the potential importance of sea or road salt resuspension by traffic. Similar urban increment values for traffic-related, resuspension and sea salt elements have been observed by Lee et al. (1994) for particles below a few micrometres. Theodosi et al. (2011) also found higher increments (> 2) for trace elements in PM_{10} aerosol from local anthropogenic sources like fossil fuel combustion (V, Ni, Cd) and traffic (Cu), relative to long-range transported Saharan dust (Fe, Mn) with increments close to 1. However, our study suggests that the non-size-resolved increment values reported in the cited studies do not fully capture the urban/rural differences.

The influence of regional transport by anthropogenically produced elements (Fig. 3) is seen by the low urban increments between 1.1 and 1.8 for P, S, K, Zn, Br, Sn and Pb in $PM_{1.0-0.3}$ ($EF > 22$) and of 1.6 for total PM_{10} mass (concentration at NK $23 \text{ } \mu\text{g m}^{-3}$, at DE $17 \text{ } \mu\text{g m}^{-3}$). The concentrations of the main components in PM_{10} (sulfate, nitrate and secondary organic compounds) within an urban area are mostly influenced by regional transport, as found in London during the REPARTEE project (Harrison et al., 2012a) and in Paris during the MEGAPOLI project (Crippa et al., 2013; Freutel et al., 2013), resulting in low increments for total PM_{10} mass. Similar urban increment values (1.3 to 1.8) for 1 and 24 h total $PM_{2.5}$ mass concentrations were reported across many sites in the UK (Harrison et al., 2012c).

4.2.2 Kerb increment

While the urban increment investigates the effect of diffuse emission sources on particle concentrations, the kerb increment investigates an urban micro-environment, specifically the local effects of roadside emissions and activities. Here, the kerb increment is calculated as the ratio of concentrations at MR to NK. However, observed concentrations at MR strongly depend on wind direction, because the road runs from approximately 260 to 80° and the street canyon with the surrounding buildings and intersections creates a complex wind circulation system (Balogun et al., 2010). Since the measurement station is located at the southern side of the canyon, measurements during time periods with winds from the south are influenced by on-road emissions on top of the urban background pollution. Higher concentrations were observed with SSE winds, i.e. perpendicular to the direction of the road by e.g. Balogun et al. (2010), Charron and Harrison (2005) and Harrison et al. (2012b).

In this study, the RDI-SR-XRF data was split into four equally spaced wind direction sectors based on wind direction data: N ($315-45^\circ$), E ($45-135^\circ$), S ($135-225^\circ$) and W ($225-315^\circ$). Figure 4 shows size-resolved trace element concentrations per wind sector normalized to the global median concentration for each element at MR. As expected, winds from the south yield the highest concentrations, whereas northern winds yield the lowest, independent of size fraction. West and east winds are parallel to the street canyon

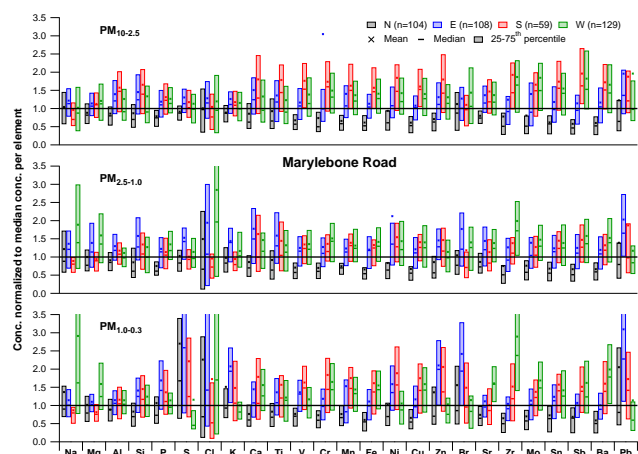


Figure 4. Mean, median and 25–75th percentile trace element concentrations at MR split in four wind direction sectors (N, E, S, W) normalized to the global median concentration per element for $PM_{10-2.5}$ (top), $PM_{2.5-1.0}$ (middle) and $PM_{1.0-0.3}$ (bottom). See Sect. 4.2.2 for the definition of the wind direction sectors.

and yield intermediate concentrations. Similar behaviour is observed for NO_x , and no directional biases for high wind speeds are observed (Fig. S6 in the Supplement).

Traffic-related and some other anthropogenically related elements (V, Cr, Mn, Fe, Ni, Cu, Zn, Zr, Mo, Sn, Sb, Ba) show the strongest wind direction dependency with up to a factor of 2–3 higher concentrations during S relative to N winds for the three size fractions (Fig. 4). A factor of 1.5–2 is obtained for resuspended dust elements. Harrison et al. (2012b) found a ratio of 2 for Fe (as tracer for brake wear) and 1.2 for Al (as tracer for mineral dust) for SW versus NE winds for particles between 2 and 3 μm . However, they were limited by their time resolution of several days, resulting in potentially substantial wind direction variations during each measurement, which would blur the different conditions and yield reduced ratios.

Other elements show only minor correlations with wind direction (Fig. 4), indicating more influence from regional transport, instead of being locally affected by traffic. Only fine mode S, K and Br seem to be enriched with winds from the east, potentially related to long-range transport from the European continent.

Local wind direction has a greatly reduced effect at urban background and rural sites. At NK, the element concentrations are only subject to high concentration outliers for E winds (Fig. S4), potentially caused by the transport of pollutants from downtown London, or by lower wind speeds occurring with E winds resulting in reduced dilution and increased concentrations of traffic pollutants (e.g. NO_x) throughout the city (Fig. S6). The rural site hardly shows wind direction dependent concentrations (Fig. S5–6). Interpretation of data from the E sector is unclear due to the low number of data points (45 out of 318 data points). Only data

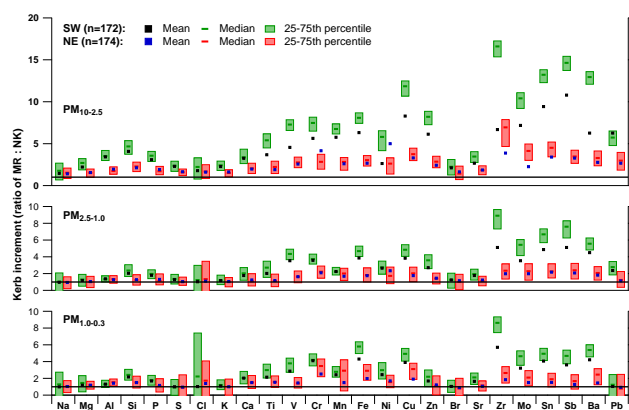


Figure 5. Mean, median and 25–75th percentile kerb increment values for trace elements at MR relative to NK for $PM_{10-2.5}$ (top), $PM_{2.5-1.0}$ (middle) and $PM_{1.0-0.3}$ (bottom) split into SW and NE wind sectors. See Sect. 4.2.2 for the definition of the wind direction sectors.

from the N sector show enhanced concentrations for several elements correlating with higher wind speeds and back trajectories consistent with transport from continental Europe.

To simplify reporting of the kerb increment and facilitate comparison with previous studies (e.g. Harrison et al., 2012b), we combined the south/west sectors and the north/east sectors into SW ($135\text{--}315^\circ$) and NE ($315\text{--}135^\circ$) sectors. To eliminate meteorological and/or regional transport effects, this segregation is performed at both MR and NK. The kerb increment is then calculated as the ratio of MR to NK and shown in Fig. 5 (Fig. S7 shows the increments for the four individual sectors). As with the urban increment, we focus on the ratio of the medians at MR and NK to reduce the effects of outliers. Two features become directly visible: the kerb increment is much higher for coarse than for intermediate and fine particles, and kerb increments are much higher for SW than for NE wind conditions. With the latter, kerb increments are on average 2.7, 1.6 and 1.7 for coarse, intermediate and fine mode particles, respectively. This significant enhancement is likely due to recirculation of particles within the street canyon following their resuspension and/or emission by traffic. However, these increments are much smaller than those observed in the SW sector, where enhancements relative to NK of 6.7, 3.3 and 3.1 (coarse, intermediate, fine) are observed. These results indicate the existence of micro-environments within the street canyon dependent on wind direction.

As in the previous discussion, we again group elements by kerb increment (Fig. 5). The first group consists of Cu, Zr, Mo, Sn, Sb and Ba and yields the highest increments in the coarse mode ranging from 10.4 to 16.6 in the SW sector (3.3–6.9 for NE). These elements are typically associated with brake wear (e.g. Bukowiecki et al., 2009b; Harrison et al., 2012b), and are much higher than the increments of 4.1 to 4.4 reported by Harrison et al. (2012b) at the same sites for

particles < 21 μm . They assigned Fe, Cu, Sb and Ba to brake wear, but in the current study Fe has a significantly lower kerb increment than other brake wear tracers, suggesting a significant alternative source. When combining all size fractions and ignoring wind direction influences, increments in this study are about 4.9, and more similar to previous studies. The discrepancies between the kerb increments obtained using these two calculation strategies highlight the difficulties in characterizing human exposure to locally generated pollutants in urban environments, as the detailed topography and microscale meteorology greatly alter particle concentrations, and the effects are size dependent. Amato et al. (2011) calculated road side increments in Barcelona for trace elements in PM_{10} with a 1 h time resolution and found increments for brake wear elements of only 1.7 (based on Fe, Cu, Sb, Cr, Sn). These low increments are probably due to the reduced dispersion in Barcelona caused by a complex topography, resulting in high urban background levels.

The second group consists of V, Cr, Mn, Fe, Ni, Zn and Pb with increments of 5.7–8.2 ($\text{PM}_{10-2.5}$) in the SW sector (2.6–3.0 for NE) (Fig. 5). V and Ni are typically assigned to industrial sources and heavy-oil combustion (e.g. Mazzei et al., 2007; Viana et al., 2008), Zn is usually associated with tyre wear (e.g. Harrison et al., 2012b; Lin et al., 2005), and the other elements are commonly associated with traffic-related emissions (e.g. Amato et al., 2013; Bukowiecki et al., 2009a; Richard et al., 2011). We label this group as anthropogenically influenced (ANTH). The EF of V, Cr and Ni are much lower than those of the other elements in this group (4 vs. > 10), indicating at least to some extent different source origins. These kerb increments are similar to the ones for NO_x of 8.5 for SW and 2.4 for NE, confirming the anthropogenic influence (traffic and other sources) on these elements. The high braking frequency at MR due to congested traffic probably resulted in increased kerb increments of brake wear relative to ANTH elements that are also influenced by local traffic and other sources around NK. Increments of these ANTH elements are higher than previously reported values of 1.8–4.5 for studies with low time resolution and non-size-segregated particles (Boogaard et al., 2011; Janssen et al., 1997). The high increments presented here might be caused by street canyon effects, trapping pollutants emitted at street level and preventing dilution to the urban background. The enhanced kerb increments for brake wear relative to ANTH elements are apparent in all three size fractions, although increments become more similar towards smaller sizes with a factor 1.7 between both element groups in the coarse, 1.5 in the intermediate and 1.4 in the fine mode. Both groups show the additional information gained with size-segregated aerosol, where exposure to trace elements in the street canyon relative to the urban background increases with particle size, either caused by increased traffic-related emissions with particle size or by more efficient transport of submicron particles from street sites to the urban background. Furthermore, the highly time-resolved element mea-

surements presented here enabled us to resolve the systematic, wind direction dependent variability in kerb increments.

The third group is associated with mineral dust (Al, Si, Ca, Ti, Sr) with coarse mode increments of 3.4–5.4 for SW winds (1.7–2.3 for NE) (Fig. 5). These elements are brought into the air both by traffic-induced resuspension and transport from other locations. This second process increases both urban background and kerbside concentrations, and thus reduces kerb increments relative to direct traffic-related elements. Lower kerb increments for mineral dust than traffic-related elements are generally observed in increment studies (Amato et al., 2011; Boogaard et al., 2011; Bukowiecki et al., 2009b; Harrison et al., 2012b), although the dust increments found in this study are larger than most reported increments (typically 1–2). As in the traffic-related groups, increments increase with particle size, indicating enhanced human exposure at the street side of particles above 1 μm .

Na, Mg and Cl (sea salt) form the fourth group and yield kerb increments of 1.0 to 2.7, independent of size fraction but with slightly enhanced ratios with SW compared to NE winds (Fig. 5). Similar increments were observed for total PM_{10} mass. As discussed for urban increments, even though these elements have regional sources, they are influenced by resuspension processes within the urban area which are enhanced at kerbside sites.

The remaining elements (P, S, K, Br) can be grouped together. In the coarse mode, these elements yield increments similar to the mineral dust group, indicating that this group is influenced by resuspension processes in the street canyon (Fig. 5). However, especially in the fine mode, increments around 1 were found, consistent with regional transport dominating over local emission sources.

4.3 Temporal trends in trace element concentrations

In contrast to traditional trace element measurements, the RDI-SR-XRF enables measurement of element concentrations with high time resolution (2 h in this work). This enables investigation of diurnal cycles, which are useful both for source discrimination and in determining the processes contributing to elevated PM levels. We also discuss weekly cycles, which can be useful in distinguishing emissions from heavy-duty and passenger vehicles (HDV and LDV); HDV numbers typically diminish during the weekend. Back trajectory analysis aids source discrimination by understanding regional transport influences by different air mass origin. Here we discuss the temporal trends of trace elements in five groups based on expected sources and the increment analyses in Sect. 4.2, in order of increasing local influence: regional background, sea salt, mineral dust, traffic-related and brake wear.

Figures 6 and 7 show size-segregated median diurnal and weekly cycles, respectively, for five elements representative of the classes mentioned above: Na (sea salt), Si (mineral dust), S (regional background), Fe (traffic-related) and

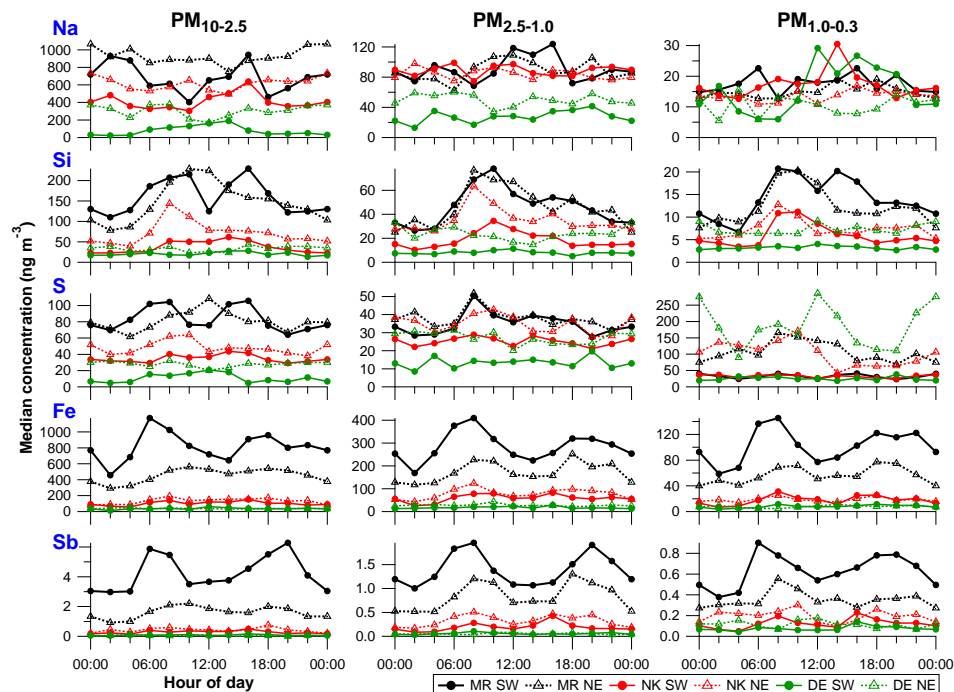


Figure 6. Diurnal cycles of 2 h median concentrations of Na, Si, S, Fe and Sb for $PM_{10-2.5}$ (left), $PM_{2.5-1.0}$ (middle) and $PM_{1.0-0.3}$ (right) at MR, NK, DE split in SW and NE wind sectors. See Sect. 4.2.2 for the definition of the wind direction sectors. Hour of day is start of 2 h sampling period, so 00:00 LT means sampling from 00:00 to 02:00 LT.

Sb (brake wear) at the three sites. Because of the wind direction effect evident at MR, diurnal cycles at all three sites are shown for SW and NE winds. Wind direction analyses are not incorporated into the weekly cycles because the month-long campaign provided insufficient data points for meaningful division. This also means that weekly cycles are subject to influences by mesoscale events. For example, sea salt shows no clear weekly cycle, except for a peak on Fridays in intermediate and fine fractions coinciding with westerly winds, which coincidentally occurred more frequently on Fridays than on other days. Except for such events, regionally dominated elements tend to display flat, featureless diurnal/weekly cycles, while elements dominated by recurring local processes (e.g. traffic patterns) show interpretable features. Diurnal and weekly cycles of all other elements can be found in Supplement Figs. S8–9. For comparison, diurnal and weekly cycles of NO_x and total PM_{10} mass at all sites, and of traffic flow at MR are shown in Fig. 8. The time series of these species were averaged to the RDI collection times before obtaining the cycles. BC diurnal and weekly cycles (not shown) are very similar to those of NO_x .

4.3.1 Regional influences

Elements dominated by regional sources (P, S, K, Br) occur mainly in the fine fraction and are similar to total PM_{10} mass in showing no obvious diurnal and weekly patterns. This interpretation is consistent with the urban/kerb increment anal-

ysis discussed in Sect. 4.2. Weekly patterns suggest fine Zn and Pb are also dominated by regional transport (Fig. S9). P, S and K have been identified as tracers for mixed wood combustion and secondary sulfate (Amato et al., 2011; Richard et al., 2011), whereas Hammond et al. (2008) have identified S, K and Pb from mixed secondary sulfate and coal combustion. Br is usually associated with sea salt (Lee et al., 1994; Mazzei et al., 2007) or traffic emissions (Gotschi et al., 2005; Lee et al., 1994), but Maenhaut (1996) has also found Br, together with S, K, Pb and other elements in biomass burning. In this study, the diurnal cycle of fine Br is different from the Na, Mg and Cl cycles, but more similar to K. The Br is thus likely more associated with wood burning than with other sources.

The time series of fine S, K, Zn, Pb at NK (very similar at MR and DE) are explored in relation to total PM_{10} mass, wind direction and air mass origin, and compared to representative elements from the other emission groups (coarse Na, Si, S, Sb; Fig. 9). Air mass origin was studied with back trajectories simulated for three case study periods (marine, European mainland and locally influenced) using the NAME model (Jones et al., 2007). Particles are released into the model atmosphere from the measurement location and their origin is tracked using meteorological fields from the Unified Model, a numerical weather prediction model. Each particle carries mass of one or more pollutant species and evolves by various physical and chemical processes during 24 h pre-

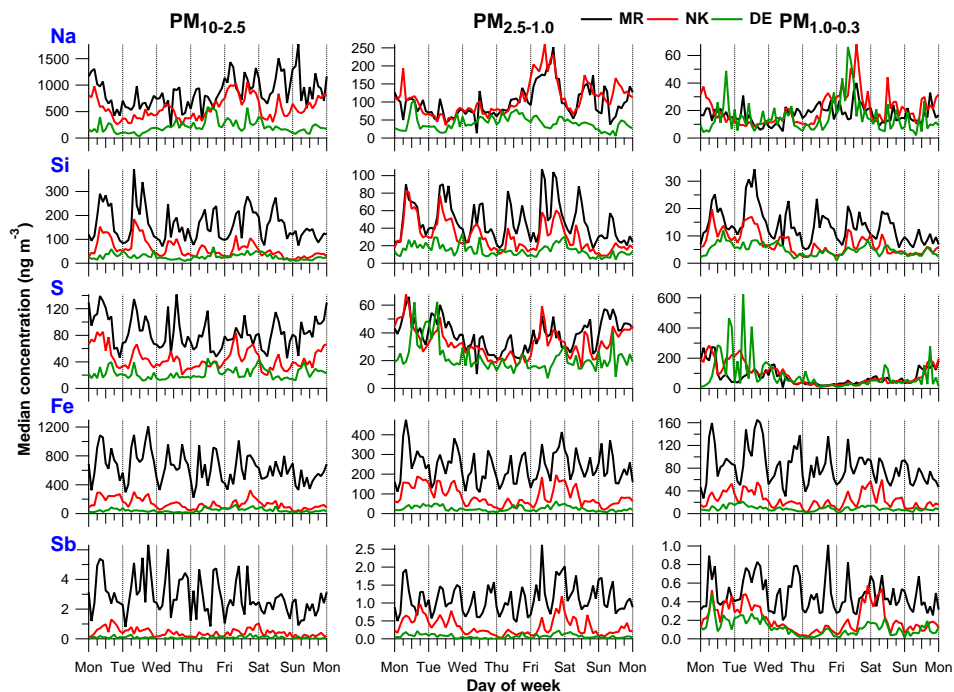


Figure 7. Weekly cycles of 2 h median concentrations of Na, Si, S, Fe and Sb for PM_{10-2.5} (left), PM_{2.5-1.0} (middle) and PM_{1.0-0.3} (right) at MR, NK, DE.

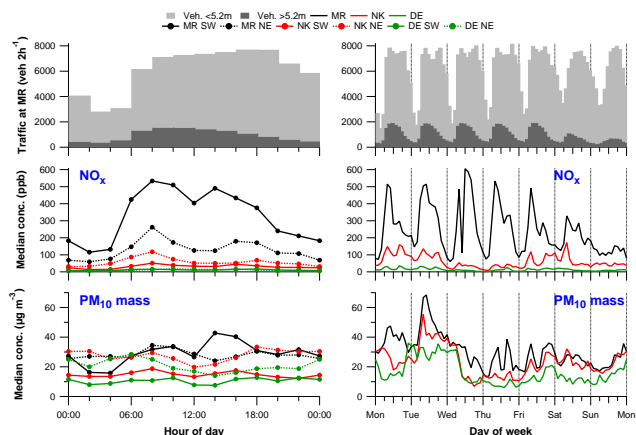


Figure 8. (top) Diurnal (left) and weekly (right) cycles of traffic flow at MR (middle and bottom left) diurnal cycles of 2 h median NO_x and total PM₁₀ mass concentrations at MR, NK and DE split into SW and NE wind sectors, and (middle and bottom right) weekly cycles of 2 h median NO_x and total PM₁₀ mass concentrations at MR, NK and DE. See Sect. 4.2.2 for the definition of the wind direction sectors. Time stamp is start of 2 h averaging period, so 00:00 LT means averaging between 00:00 and 02:00 LT.

ceding arrival at NK. Potential emission source regions can be highlighted along the pathway to the measurement site at 0–100 m above ground.

Under marine air mass origin (case A, 18–24 January, Fig. 9) with strong W winds the concentrations of the fine

mode elements are fairly low, whereas sea salt concentrations are enhanced (see Na in Fig. 9). Although the air mass has also passed over Ireland and the Midlands, the influence of these rather sparsely populated regions on pollution levels seems small. This is confirmed by low total PM₁₀ mass and NO_x concentrations. Enhanced fine fraction and total PM₁₀ mass concentrations (latter not shown) occur during north-easterlies with high wind speeds from the European mainland (case B) bringing in pollutants through regional transport.

During this episode, both the urban background and rural site observed the highest concentrations for these trace elements of the entire campaign. Traffic-influenced species were not enhanced during this pollution episode. Elevated concentrations of all trace elements, NO_x and PM₁₀ mass occurred only during a local pollution episode of roughly 3 days caused by local air mass stagnation over London and the southeastern UK (case C). The very high concentrations observed in case B through regional transport from the European mainland were identified as the main reason for PM₁₀ limit exceedances at urban background sites in London by Charron et al. (2007), while exceedances were much less frequent under marine-influenced air as represented by case A in this study.

4.3.2 Sea salt

The sea salt group yields comparable, rather flat diurnal cycles for fine and intermediate mode Na, Mg and Cl, and coarse mode Na and Cl (Na in Fig. 6; others in Supplement

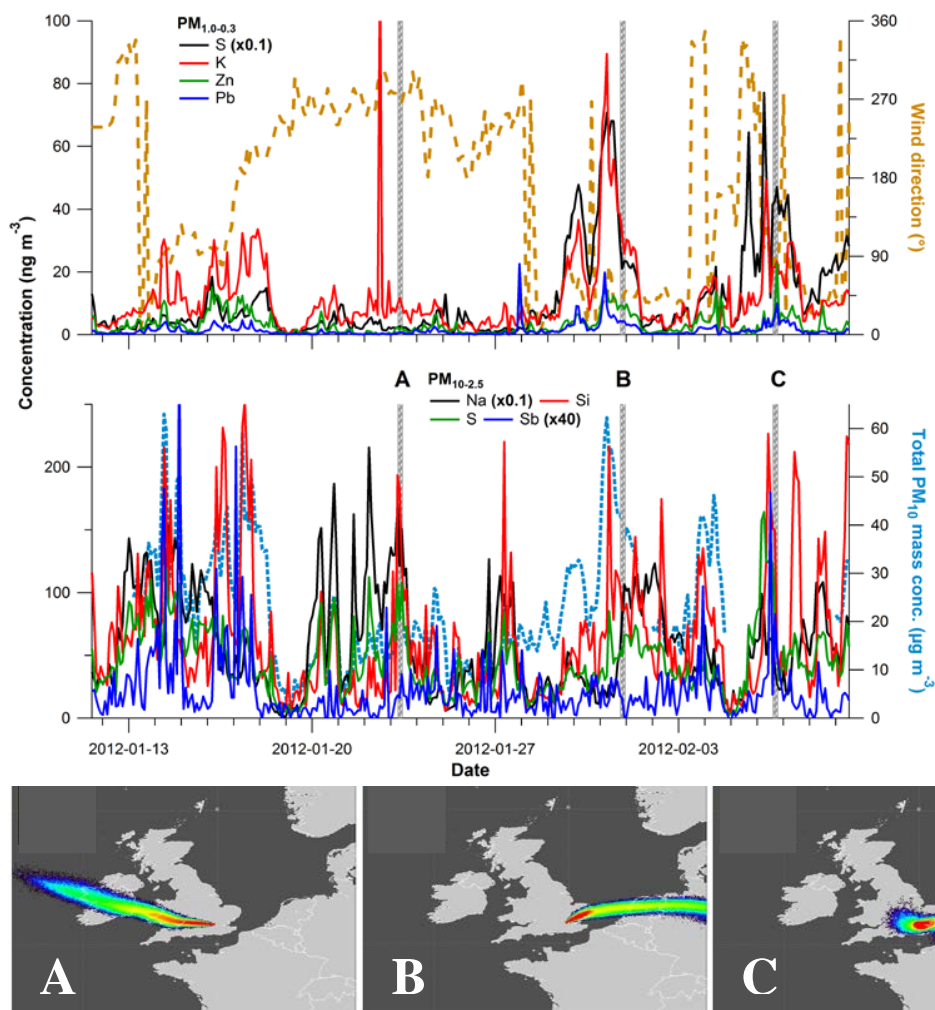


Figure 9. Top panel: time series of (top left axis) $PM_{1.0-0.3}$ S, K, Zn and Pb concentrations at NK and (top right axis) wind direction from BT Tower, time series of (bottom left axis) $PM_{10-2.5}$ Na, Si, S and Sb concentrations at NK and (bottom right axis) total PM_{10} mass concentration at NK; bottom panel: three NK footprints simulated with the NAME model corresponding to the vertical lines (A, B, C) indicated in the top panel. Trajectories are simulated for particles released from NK and followed back at 0–100 m a.g.l. for the previous 24 h at: (a) 23 January 2012 09:00 LT, (b) 31 January 2012 21:00 LT, (c) 6 February 2012 18:00 LT; particle concentrations increase from blue to red.

Fig. S8), and no obvious weekly patterns (Na in Fig. 7; others in Supplement Fig. S9). This indicates that the regional transport of sea salt is probably the main source of Na, Mg and Cl, as seen in case A in Fig. 9.

Interestingly, although coarse mode sea salt exhibits no obvious temporal trend, the urban and kerb increments indicate additional source contributions besides regional transported sea salt. The urban increment might be caused by the natural sea salt gradient observed in the UK, with reducing concentrations from west to east (Fowler and Smith, 2000), while the kerb increment could be the result of road salt resuspension in addition to sea salt resuspension. Coarse mode Mg originates probably both from mineral dust and sea salt, because at MR with SW winds Mg correlates with Al and Si

temporal trends, while with NE winds Mg correlates better with Na and Cl.

4.3.3 Mineral dust and traffic

Both mineral dust and traffic-related elements are strongly influenced by traffic patterns at MR, which are shown in Fig. 8 as the number of vehicles per 2 h split in LDV and HDV (shorter/longer than 5.2 m). HDV numbers peak in the morning, whereas LDV numbers peak in the evening when the flow of traffic leaves the urban area, consistent with Harrison et al. (2012b). A single peak during midday in the weekend compared to a double peak at weekdays is observed for LDV; HDV numbers show a similar pattern during weekdays, but with a reduced maximum on Saturday and a small

maximum that is shifted towards midday on Sunday. Charron and Harrison (2005) reported similar traffic patterns during 2 years of traffic counts, and very small week-to-week variability, except during holidays.

The element diurnal (Fig. 6 for Si, Fe and Sb; Supplement Fig. S8 for others) and weekly (Fig. 7 for Si, Fe and Sb; Supplement Fig. S9 for others) cycles yield highest concentrations at MR and lower concentrations at NK and DE, consistent with observed urban and kerb increments. More importantly, and only retrievable with high time-resolved data, concentrations are higher during the day than at night, with night time concentrations at MR and NK similar to median urban background and rural concentrations, respectively, demonstrating the effects of local traffic and enhanced human exposure during daytime. Weekdays yield stronger increments than weekends and closely follow NO_x and HDV traffic patterns (Fig. 8), indicating the strong influence of these vehicles on element concentrations. This confirms observations by Charron et al. (2007), who stated that PM_{10} limit exceedances at MR are more likely to occur on weekdays, in combination with large regional contributions from the European mainland with easterly winds. Similarly, Barmpadimos et al. (2011) found strong weekly cycles for $\text{PM}_{10-2.5}$ and $\text{PM}_{2.5}$ mass concentrations in Switzerland over a 7–12 year period, with higher concentrations on weekdays and lowest on Sundays.

In the street canyon with SW winds, all coarse mode elements (including dust elements) except Na and Cl exhibit a double peak in the diurnal cycles, closely following the flow of traffic and confirming that traffic-related processes such as braking and resuspension dominate the concentration of most elements. With NE winds, source discrimination is possible between mineral dust (Si in Fig. 6) and traffic-related elements (Fe and Sb in Fig. 6). Mineral dust yields a strong maximum between 08:00 and 14:00 LT, and continued high concentrations throughout the day, while the traffic-related group yields a reduced double peak relative to SW winds. The increase in dust concentrations coincides with the start of traffic flows at 06:00 LT resulting in resuspension of particles within the street canyon. However, concentrations decrease before traffic flows reduce, possibly as a result of increased mixing and dilution during boundary layer growth. At NK diurnal and weekly patterns of the dust and traffic groups yield similar variability but reduced concentrations relative to MR, which suggests increased human exposure during day time and weekdays and confirms that traffic dominates urban background element concentrations in London (see Dore et al., 2003). At DE, freshly emitted pollutants from London and other cities in the southeastern UK have been diluted and mixed with other pollutants during their transport to the rural background, resulting in no obvious diurnal and weekly patterns independent of size range.

The kerb increments at MR under SW winds were divided into two traffic-related groups: brake wear and other traffic-related elements. However, the diurnal and weekly cycles of

all these elements correlate well and no obvious split into two groups is seen. Apparently, both groups are co-emitted as a single group under comparable vehicle fleet and/or set of driving conditions, at least on a 2 h timescale, but in different ratios at MR and NK. The ratio of these two element classes for SW to NE wind sectors at MR is almost 2, with the lack of difference between these classes supporting co-emission. In a future paper we will further explore the diurnal variability of emission sources at both sites with statistical analyses based on the Multilinear Engine (Canonaco et al., 2013; Paatero, 1999).

5 Conclusions

Aerosol trace element composition was measured at kerbside, urban background and rural sites in the European megacity of London during winter 2012. Sampling with rotating drum impactors (RDIs) and subsequent measurements with synchrotron radiation-induced X-ray fluorescence spectrometry (SR-XRF) yielded trace element mass concentrations in $\text{PM}_{10-2.5}$, $\text{PM}_{2.5-1.0}$ and $\text{PM}_{1.0-0.3}$ aerosol with a 2 h time resolution. Total median element mass concentrations of 4.1, 2.1 and $1.0 \mu\text{g m}^{-3}$ were found at kerbside, urban background and rural sites, respectively, being 14 % of total PM_{10} mass (highest at kerbside; lowest at rural site), neglecting the corresponding oxides. The contribution of emission sources to coarse fraction elements was on average largest at kerbside (65 %) and reduced for urban background (52 %) and rural sites (49 %).

Urban and kerb increments were defined as the concentration ratios of urban background to rural, and kerbside-to-urban background, respectively, and the kerb increments were further explored as a function of wind direction. The group with the largest kerb increments consisted of elements typically associated with brake wear (Cu, Zr, Mo, Sn, Sb, Ba). The second largest kerb increments were observed for anthropogenically influenced elements typically assigned to non-brake wear traffic emissions (Cr, Mn, Fe, Zn, Pb) but also V and Ni. This could indicate either a traffic source for these elements or a similar kerbside-to-urban emission gradient. Kerb increments were larger for the brake wear group and under SW winds due to local street canyon effects, with coarse fraction increments between 10.4 and 16.6 for SW winds (3.3–6.9 for NE winds) against increments for the anthropogenically influenced group between 5.7 and 8.2 for SW winds (2.6–3.0 for NE winds). The kerb increments for all these elements in the $\text{PM}_{10-2.5}$ size fraction are roughly twice that of the $\text{PM}_{1.0-0.3}$ fraction. Urban increments (no distinction between both groups) were around 3.0. In addition to direct emissions, traffic-related processes influence the concentrations of other elements by resuspension, with mineral dust (Al, Si, Ca, Ti, Sr) increments of 1.3–3.3.

The highly time-resolved data enabled studying diurnal patterns. The cycles of mineral dust elements and coarse Na, Mg and Cl both indicate major concentration enhance-

ments during periods of heavy traffic, whereas regionally influenced elements (fine P, S, K, Zn, Br, Pb) showed no enhancements. All traffic-related elements at the kerbside site yielded temporal patterns similar to variations in heavy duty vehicle numbers as opposed to total vehicle numbers, and resulted in enhanced exposure to elements during day time and weekdays. Traffic-related processes therefore exhibit a dominant influence on air quality at the kerbside and urban background sites, and should be the main focus of health effect studies and mitigation strategies. With technological improvements for the reduction of traffic exhaust emissions, the traffic contribution to coarse PM is becoming more important as shown by decreasing PM_{2.5} mass trends with no significant changes of coarse PM (Barmpadimos et al., 2012).

Trace element and total PM₁₀ mass concentrations are also affected by mesoscale meteorology, increasing with the transport of air masses from the European mainland. Under these conditions, coarse and intermediate fraction trace elements are hardly affected, but fine fraction elements showed elevated concentrations. Trace element concentrations in London are therefore influenced by both local and regional sources, with coarse and intermediate fractions dominated by anthropogenic activities (particularly traffic-induced resuspension and wearing processes), whereas fine fractions are significantly influenced by regional processes.

These observations highlight both the strong influence of regional factors on overall air quality, as well as the need for detailed characterization of urban micro-environments for accurate assessment of human exposure to airborne particulates and the associated health risks.

The Supplement related to this article is available online at doi:10.5194/acp-15-2367-2015-supplement.

Acknowledgements. This research, which was conducted in the context of the ClearLo project, is mainly financed by the Swiss National Science Foundation (SNSF grant 200021_132467/1), the ClearLo project (NERC grant NE/H00324X/1) and the European Community's Seventh Framework Programme (FP/2007-2013, grant number 312284). The Detling site was supported by the US Department of Energy Atmospheric Systems Research Program (DOE Award No. DE-SC0006002). J. G. Slowik acknowledges support from the SNSF through the Ambizione program (grant PX00P2_31673). Filter digestions were carried out by the wet geochemistry laboratory at Royal Holloway, University of London. Empa loaned us a RDI during the ClearLo project. Parts of the work were carried out at the Swiss Light Source, Paul Scherrer Institute, Villigen, Switzerland. We thank Andreas Jaggi for technical support at the beamline X05DA. Parts were performed at the light source facility DORIS III at HASYLAB/DESY. DESY is a member of the Helmholtz Association (HGF). We thank Christophe Frieß for excellent support in acquiring and testing the detector, and we thank Peter Lienemann and Sylvia Köchli for valuable input for the production of calibration standards.

Edited by: W. Maenhaut

References

- Amato, F., Pandolfi, M., Escrig, A., Querol, X., Alastuey, A., Pey, J., Perez, N., and Hopke, P. K.: Quantifying road dust resuspension in urban environment by Multilinear Engine: A comparison with PMF2, *Atmos. Environ.*, 43, 2770–2780, 2009.
- Amato, F., Viana, M., Richard, A., Furger, M., Prévôt, A. S. H., Nava, S., Lucarelli, F., Bukowiecki, N., Alastuey, A., Reche, C., Moreno, T., Pandolfi, M., Pey, J., and Querol, X.: Size and time-resolved roadside enrichment of atmospheric particulate pollutants, *Atmos. Chem. Phys.*, 11, 2917–2931, doi:10.5194/acp-11-2917-2011, 2011.
- Amato, F., Schaap, M., Denier van der Gon, H. A. C., Pandolfi, M., Alastuey, A., Keuken, M., and Querol, X.: Short-term variability of mineral dust, metals and carbon emission from road dust resuspension, *Atmos. Environ.*, 74, 134–140, 2013.
- Arnold, S. J., ApSimon, H., Barlow, J., Belcher, S., Bell, M., Boddy, J. W., Britter, R., Cheng, H., Clark, R., Colville, R. N., Dimitroulopoulou, S., Dobre, A., Grealley, B., Kaur, S., Knights, A., Lawton, T., Makepeace, A., Martin, D., Neophytou, M., Neville, S., Nieuwenhuijsen, M., Nickless, G., Price, C., Robins, A., Shallcross, D., Simmonds, P., Smalley, R. J., Tate, J., Tomlin, A. S., Wang, H., and Walsh, P.: Introduction to the DAPPLE Air Pollution Project, *Sci. Total Environ.*, 332, 139–153, 2004.
- Balogun, A. A., Tomlin, A. S., Wood, C. R., Barlow, J. F., Belcher, S. E., Smalley, R. J., Lingard, J. J. N., Arnold, S. J., Dobre, A., Robins, A. G., Martin, D., and Shallcross, D. E.: In-street wind direction variability in the vicinity of a busy intersection in central London, *Bound.-Lay. Meteorol.*, 136, 489–513, doi:10.1007/s10546-010-9515-y, 2010.
- Barmpadimos, I., Nufer, M., Oderbolz, D. C., Keller, J., Aksoyoglu, S., Hueglin, C., Baltensperger, U., and Prévôt, A. S. H.: The weekly cycle of ambient concentrations and traffic emissions of coarse (PM₁₀–PM_{2.5}) atmospheric particles, *Atmos. Environ.*, 45, 4580–4590, 2011.
- Barmpadimos, I., Keller, J., Oderbolz, D., Hueglin, C., and Prévôt, A. S. H.: One decade of parallel fine (PM_{2.5}) and coarse (PM₁₀–PM_{2.5}) particulate matter measurements in Europe: trends and variability, *Atmos. Chem. Phys.*, 12, 3189–3203, doi:10.5194/acp-12-3189-2012, 2012.
- Bigi, A. and Harrison, R. M.: Analysis of the air pollution climate at a central urban background site, *Atmos. Environ.*, 44, 2004–2012, 2010.
- Bohnenstengel, S. I., Evans, S., Clark, P. A., and Belcher, S. E.: Simulations of the London urban heat island, *Q. J. Roy. Meteor. Soc.*, 137, 1625–1640, doi:10.1002/qj.855, 2011.
- Bohnenstengel, S. I., Hamilton, I., Davies, M., and Belcher, S. E.: Impact of anthropogenic heat emissions on London's temperatures, *Q. J. Roy. Meteor. Soc.*, doi:10.1002/qj.2144, 2013.
- Bohnenstengel, S. I., Belcher, S. E., Aiken, A., Allan, J. D., Allen, G., Bacak, A., Bannan, T. J., Barlow, J. F., Beddows, D. C. S., Bloss, W. J., Booth, A. M., Chemel, C., Coceal, O., Di Marco, C. F., Dubey, M. K., Faloon, K. H., Fleming, Z. L., Furger, M., Gietl, J. K., Graves, R. R., Green, D. C., Grimmond, C. S. B., Halios, C. H., Hamilton, J. F., Harrison, R. M., Heal, M. R., Heard, D. E., Helfter, C., Herndon, S. C., Holmes, R. E., Hopkins, J. R., Jones, A. M., Kelly, F. J., Kotthaus, S., Langford, B., Lee, J. D., Leigh, R. J., Lewis, A. C., Lidster, R. T., Lopez-Hilfiker, F. D., McQuaid, J. B., Mohr, C., Monks, P. S., Nemitz, E., Ng, N. L., Percival, C. J., Prévôt, A. S. H., Ricketts, H. M. A., Sokhi, R.,

- Stone, D., Thornton, J. A., Tremper, A. H., Valach, A. C., Visser, S., Whalley, L. K., Williams, L. R., Xu, L., Young, D. E., and Zotter, P.: Meteorology, air quality, and health in London: The ClearLo project, *B. Am. Meteorol. Soc.*, doi:10.1175/bams-d-12-00245.1, 2014.
- Boogaard, H., Kos, G. P. A., Weijers, E. P., Janssen, N. A. H., Fischer, P. H., van der Zee, S. C., de Hartog, J. J., and Hoek, G.: Contrast in air pollution components between major streets and background locations: Particulate matter mass, black carbon, elemental composition, nitrogen oxide and ultrafine particle number, *Atmos. Environ.*, 45, 650–658, 2011.
- Bukowiecki, N., Hill, M., Gehrig, R., Zwicky, C. N., Lienemann, P., Hegedus, F., Falkenberg, G., Weingartner, E., and Baltensperger, U.: Trace metals in ambient air: Hourly size-segregated mass concentrations determined by synchrotron-XRF, *Environ. Sci. Technol.*, 39, 5754–5762, 2005.
- Bukowiecki, N., Lienemann, P., Zwicky, C. N., Furger, M., Richard, A., Falkenberg, G., Rickers, K., Grolimund, D., Borca, C., Hill, M., Gehrig, R., and Baltensperger, U.: X-ray fluorescence spectrometry for high throughput analysis of atmospheric aerosol samples: The benefits of synchrotron X-rays, *Spectrochim. Acta B*, 63, 929–938, 2008.
- Bukowiecki, N., Gehrig, R., Lienemann, P., Hill, M., Figi, R., Buchmann, B., Furger, M., Richard, A., Mohr, C., Weimer, S., Prevot, A. S. H., and Baltensperger, U.: PM₁₀ emission factors of abrasion particles from road traffic, *Schweizerische Eidgenossenschaft*, 2009a.
- Bukowiecki, N., Lienemann, P., Hill, M., Figi, R., Richard, A., Furger, M., Rickers, K., Falkenberg, G., Zhao, Y. J., Cliff, S. S., Prevot, A. S. H., Baltensperger, U., Buchmann, B., and Gehrig, R.: Real-world emission factors for antimony and other brake wear related trace elements: Size-segregated values for light and heavy duty vehicles, *Environ. Sci. Technol.*, 43, 8072–8078, 2009b.
- Bukowiecki, N., Richard, A., Furger, M., Weingartner, E., Aguirre, M., Huthwelker, T., Lienemann, P., Gehrig, R., and Baltensperger, U.: Deposition uniformity and particle size distribution of ambient aerosol collected with a rotating drum impactor, *Aerosol Sci. Tech.*, 43, 891–901, 2009c.
- Bukowiecki, N., Lienemann, P., Hill, M., Furger, M., Richard, A., Amato, F., Prevot, A. S. H., Baltensperger, U., Buchmann, B., and Gehrig, R.: PM₁₀ emission factors for non-exhaust particles generated by road traffic in an urban street canyon and along a freeway in Switzerland, *Atmos. Environ.*, 44, 2330–2340, 2010.
- Calzolari, G., Chiari, M., Lucarelli, F., Nava, S., and Portarena, S.: Proton induced gamma-ray emission yields for the analysis of light elements in aerosol samples in an external beam set-up, *Nucl. Instrum. Meth. B*, 268, 1540–1545, 2010.
- Canonaco, F., Crippa, M., Slowik, J. G., Baltensperger, U., and Prévôt, A. S. H.: SoFi, an IGOR-based interface for the efficient use of the generalized multilinear engine (ME-2) for the source apportionment: ME-2 application to aerosol mass spectrometer data, *Atmos. Meas. Tech.*, 6, 3649–3661, doi:10.5194/amt-6-3649-2013, 2013.
- Charron, A. and Harrison, R. M.: Fine (PM_{2.5}) and coarse (PM_{2.5}–PM₁₀) particulate matter on a heavily trafficked London highway: Sources and processes, *Environ. Sci. Technol.*, 39, 7768–7776, doi:10.1021/es050462i, 2005.
- Charron, A., Harrison, R. M., and Quincey, P.: What are the sources and conditions responsible for exceedences of the 24h PM₁₀ limit value (50 µg m⁻³) at a heavily trafficked London site?, *Atmos. Environ.*, 41, 1960–1975, 2007.
- Crippa, M., DeCarlo, P. F., Slowik, J. G., Mohr, C., Heringa, M. F., Chirico, R., Poulain, L., Freutel, F., Sciare, J., Cozic, J., Di Marco, C. F., Elsasser, M., Nicolas, J. B., Marchand, N., Abidi, E., Wiedensohler, A., Drewnick, F., Schneider, J., Borrmann, S., Nemitz, E., Zimmermann, R., Jaffrezo, J.-L., Prévôt, A. S. H., and Baltensperger, U.: Wintertime aerosol chemical composition and source apportionment of the organic fraction in the metropolitan area of Paris, *Atmos. Chem. Phys.*, 13, 961–981, doi:10.5194/acp-13-961-2013, 2013.
- DeCarlo, P. F., Kimmel, J. R., Trimborn, A., Northway, M. J., Jayne, J. T., Aiken, A. C., Gonin, M., Fuhrer, K., Horvath, T., Docherty, K. S., Worsnop, D. R., and Jimenez, J. L.: Field-deployable, high-resolution, time-of-flight aerosol mass spectrometer, *Anal. Chem.*, 78, 8281–8289, doi:10.1021/ac061249n, 2006.
- Dockery, D. W. and Pope, C. A., III: Acute respiratory effects of particulate air pollution, in: *Annual Review of Public Health*, edited by: Omenn, G. S., *Annual Review of Public Health*, Annual Reviews Inc., P.O. Box 10139, 4139 El Camino Way, Palo Alto, California 94306, USA, 107–132, 1994.
- Dore, C. J., Goodwin, J. W. L., Watterson, J. D., Murrels, T. P., Passant, N. R., Hobson, M. M., Haigh, K. E., Baggott, S. L., Pye, S. T., Coleman, P. J., and King, K. R.: UK Emissions of Air Pollutants 1970 to 2001, *National Atmospheric Emissions Inventory*, 2003.
- Flechsigg, U., Jaggi, A., Spielmann, S., Padmore, H. A., and MacDowell, A. A.: The optics beamline at the Swiss Light Source, *Nucl. Instrum. Meth. A*, 609, 281–285, 2009.
- Formenti, P., Prati, P., Zucchiatti, A., Lucarelli, F., and Mando, P. A.: Aerosol study in the town of Genova with a PIXE analysis, *Nucl. Instrum. Meth. B*, 113, 359–362, 1996.
- Formenti, P., Nava, S., Prati, P., Chevaillier, S., Klaver, A., Lafon, S., Mazzei, F., Calzolari, G., and Chiari, M.: Self-attenuation artifacts and correction factors of light element measurements by X-ray analysis: Implication for mineral dust composition studies, *J. Geophys. Res.-Atmos.*, 115, 8 pp., doi:10.1029/2009jd012701, 2010.
- Fowler, D. and Smith, R.: Spatial and temporal variability in the deposition of acidifying species in the UK between 1986 and 1997, *Department of Environment, Food and Rural Affairs*, 2000.
- Franklin, M., Koutrakis, P., and Schwartz, J.: The role of particle composition on the association between PM_{2.5} and mortality, *Epidemiology*, 19, 680–689, doi:10.1097/ede.0b013e3181812bb7, 2008.
- Freutel, F., Schneider, J., Drewnick, F., von der Weiden-Reinmüller, S.-L., Crippa, M., Prévôt, A. S. H., Baltensperger, U., Poulain, L., Wiedensohler, A., Sciare, J., Sarda-Estève, R., Burkhardt, J. F., Eckhardt, S., Stohl, A., Gros, V., Colomb, A., Michoud, V., Doussin, J. F., Borbon, A., Haeffelin, M., Morille, Y., Beekmann, M., and Borrmann, S.: Aerosol particle measurements at three stationary sites in the megacity of Paris during summer 2009: meteorology and air mass origin dominate aerosol particle composition and size distribution, *Atmos. Chem. Phys.*, 13, 933–959, doi:10.5194/acp-13-933-2013, 2013.
- Gotschi, T., Hazenkamp-Von Arxb, M. E., Heinrich, J., Bono, R., Burney, P., Forsberg, B., Jarvis, D., Maldonado, J., Norback,

- D., Stern, W. B., Sunyer, J., Toren, K., Verlato, G., Villani, S., and Kunzli, N.: Elemental composition and reflectance of ambient fine particles at 21 European locations, *Atmos. Environ.*, 39, 5947–5958, 2005.
- Hammond, D. M., Dvonch, J. T., Keeler, G. J., Parker, E. A., Kamal, A. S., Barres, J. A., Yip, F. Y., and Brakefield-Caldwell, W.: Sources of ambient fine particulate matter at two community sites in Detroit, Michigan, *Atmos. Environ.*, 42, 720–732, 2008.
- Harrison, R. M. and Jones, A. M.: Multisite study of particle number concentrations in urban air, *Environ. Sci. Technol.*, 39, 6063–6070, doi:10.1021/es040541e, 2005.
- Harrison, R. M., Yin, J., Mark, D., Stedman, J., Appleby, R. S., Booker, J., and Moorcroft, S.: Studies of the coarse particle (2.5–10 μm) component in UK urban atmospheres, *Atmos. Environ.*, 35, 3667–3679, 2001.
- Harrison, R. M., Stedman, J., and Derwent, D.: New Directions: Why are PM_{10} concentrations in Europe not falling?, *Atmos. Environ.*, 42, 603–606, 2008.
- Harrison, R. M., Beddows, D. C. S., and Dall'Osto, M.: PMF analysis of wide-range particle size spectra collected on a major highway, *Environ. Sci. Technol.*, 45, 5522–5528, 2011.
- Harrison, R. M., Dall'Osto, M., Beddows, D. C. S., Thorpe, A. J., Bloss, W. J., Allan, J. D., Coe, H., Dorsey, J. R., Gallagher, M., Martin, C., Whitehead, J., Williams, P. I., Jones, R. L., Langridge, J. M., Benton, A. K., Ball, S. M., Langford, B., Hewitt, C. N., Davison, B., Martin, D., Petersson, K. F., Henshaw, S. J., White, I. R., Shallcross, D. E., Barlow, J. F., Dunbar, T., Davies, F., Nemitz, E., Phillips, G. J., Helfter, C., Di Marco, C. F., and Smith, S.: Atmospheric chemistry and physics in the atmosphere of a developed megacity (London): an overview of the REPARTEE experiment and its conclusions, *Atmos. Chem. Phys.*, 12, 3065–3114, doi:10.5194/acp-12-3065-2012, 2012a.
- Harrison, R. M., Jones, A. M., Gietl, J., Yin, J., and Green, D. C.: Estimation of the contributions of brake dust, tire wear, and resuspension to nonexhaust traffic particles derived from atmospheric measurements, *Environ. Sci. Technol.*, 46, 6523–6529, doi:10.1021/es300894r, 2012b.
- Harrison, R. M., Laxen, D., Moorcroft, S., and Laxen, K.: Processes affecting concentrations of fine particulate matter ($\text{PM}_{2.5}$) in the UK atmosphere, *Atmos. Environ.*, 46, 115–124, 2012c.
- Janssen, N. A. H., Van Mansom, D. F. M., Van Der Jagt, K., Harssema, H., and Hoek, G.: Mass concentration and elemental composition of airborne particulate matter at street and background locations, *Atmos. Environ.*, 31, 1185–1193, 1997.
- Jones, A. M., Harrison, R. M., and Baker, J.: The wind speed dependence of the concentrations of airborne particulate matter and NO_x , *Atmos. Environ.*, 44, 1682–1690, 2010.
- Jones, A. R., Thomson, D. J., Hort, M., and Devenish, B.: The UK Met Office's next-generation atmospheric dispersion model, NAME III, Air Pollution Modeling and its Application XVII, edited by: Borrego, C., and Norman, A.-L., Springer, Exeter, UK, 2007.
- Kelly, F. J. and Fussell, J. C.: Size, source and chemical composition as determinants of toxicity attributable to ambient particulate matter, *Atmos. Environ.*, 60, 504–526, 2012.
- Lee, D. S., Garland, J. A., and Fox, A. A.: Atmospheric concentrations of trace elements in urban areas of the United Kingdom, *Atmos. Environ.*, 28, 2691–2713, 1994.
- Lenschow, P., Abraham, H. J., Kutzner, K., Lutz, M., Preuß, J. D., and Reichenbacher, W.: Some ideas about the sources of PM_{10} , *Atmos. Environ.*, 35, Supplement 1, S23–S33, doi:10.1016/S1352-2310(01)00122-4, 2001.
- Lin, C. C., Chen, S. J., Huang, K. L., Hwang, W. I., Chang-Chien, G. P., and Lin, W. Y.: Characteristics of metals in nano/ultrafine/fine/coarse particles collected beside a heavily trafficked road, *Environ. Sci. Technol.*, 39, 8113–8122, 2005.
- Lucarelli, F., Mando, P. A., Nava, S., Valerio, M., Prati, P., and Zucchiatti, A.: Elemental composition of urban aerosol collected in Florence, Italy, *Environ. Monit. Assess.*, 65, 165–173, 2000.
- Maenhaut, W.: "Global Change" related and other atmospheric aerosol research at the University of Gent, and the role of PIXE therein, *Nucl. Instrum. Meth. B*, 109, 419–428, 1996.
- Mavrogiani, A., Davies, M., Batty, M., Belcher, S. E., Bohnenstengel, S. I., Carruthers, D., Chalabi, Z., Croxford, B., Demanuele, C., Evans, S., Giridharan, R., Hacker, J. N., Hamilton, I., Hogg, C., Hunt, J., Kolokotroni, M., Martin, C., Milner, J., Rajapaksha, I., Ridley, I., Steadman, J. P., Stocker, J., Wilkinson, P., and Ye, Z.: The comfort, energy and health implications of London's urban heat island, *Build Serv. Eng. Res. T.*, 32, 35–52, doi:10.1177/0143624410394530, 2011.
- Mazzei, F., Lucarelli, F., Nava, S., Prati, P., Valli, G., and Vecchi, R.: A new methodological approach: The combined use of two-stage streaker samplers and optical particle counters for the characterization of airborne particulate matter, *Atmos. Environ.*, 41, 5525–5535, 2007.
- Minguillón, M. C., Cirach, M., Hoek, G., Brunekreef, B., Tsai, M., de Hoogh, K., Jedynska, A., Kooter, I. M., Nieuwenhuijsen, M., and Querol, X.: Spatial variability of trace elements and sources for improved exposure assessment in Barcelona, *Atmos. Environ.*, 89, 268–281, 2014.
- Moffet, R. C., Desyaterik, Y., Hopkins, R. J., Tivanski, A. V., Gilles, M. K., Wang, Y., Shutthanandan, V., Molina, L. T., Abraham, R. G., Johnson, K. S., Mugica, V., Molina, M. J., Laskin, A., and Prather, K. A.: Characterization of aerosols containing Zn, Pb, and Cl from an industrial region of Mexico City, *Environ. Sci. Technol.*, 42, 7091–7097, 2008.
- Mohr, C., Lopez-Hilfiker, F. D., Zotter, P., Prévôt, A. S. H., Xu, L., Ng, N. L., Herndon, S. C., Williams, L. R., Franklin, J. P., Zahniser, M. S., Worsnop, D. R., Knighton, W. B., Aiken, A. C., Gorkowski, K. J., Dubey, M. K., Allan, J. D., and Thornton, J. A.: Contribution of nitrated phenols to wood burning brown carbon light absorption in Detling, United Kingdom during winter time, *Environ. Sci. Technol.*, 47, 6316–6324, doi:10.1021/es400683v, 2013.
- Moreno, T., Karanasiou, A., Amato, F., Lucarelli, F., Nava, S., Calzolari, G., Chiari, M., Coz, E., Artinano, B., Lumberras, J., Borge, R., Boldo, E., Linares, C., Alastuey, A., Querol, X., and Gibbons, W.: Daily and hourly sourcing of metallic and mineral dust in urban air contaminated by traffic and coal-burning emissions, *Atmos. Environ.*, 68, 33–44, doi:10.1016/j.atmosenv.2012.11.037, 2013.
- Nolte, C. G., Bhave, P. V., Arnold, J. R., Dennis, R. L., Zhang, K. M., and Wexler, A. S.: Modeling urban and regional aerosols – Application of the CMAQ-UCD Aerosol Model to Tampa, a coastal urban site, *Atmos. Environ.*, 42, 3179–3191, 2008.
- Paatero, P.: The multilinear engine – A table-driven, least squares program for solving multilinear problems, including the n-way

- parallel factor analysis model, *J. Comput. Graph. Stat.*, 8, 854–888, doi:10.1080/10618600.1999.10474853, 1999.
- Putaud, J. P., Van Dingenen, R., Alastuey, A., Bauer, H., Birmili, W., Cyrys, J., Flentje, H., Fuzzi, S., Gehrig, R., Hansson, H. C., Harrison, R. M., Herrmann, H., Hitzenberger, R., Hüglin, C., Jones, A. M., Kasper-Giebl, A., Kiss, G., Koussa, A., Kuhlbusch, T. A. J., Löschau, G., Maenhaut, W., Molnar, A., Moreno, T., Pekkanen, J., Perrino, C., Pitz, M., Puxbaum, H., Querol, X., Rodriguez, S., Salma, I., Schwarz, J., Smolik, J., Schneider, J., Spindler, G., ten Brink, H., Tursic, J., Viana, M., Wiedensohler, A., and Raes, F.: A European aerosol phenomenology – 3: Physical and chemical characteristics of particulate matter from 60 rural, urban, and kerbside sites across Europe, *Atmos. Environ.*, 44, 1308–1320, 2010.
- Querol, X., Viana, M., Alastuey, A., Amato, F., Moreno, T., Castillo, S., Pey, J., de la Rosa, J., Sánchez de la Campa, A., Artñiano, B., Salvador, P., García Dos Santos, S., Fernández-Patier, R., Moreno-Grau, S., Negral, L., Minguillón, M. C., Monfort, E., Gil, J. I., Inza, A., Ortega, L. A., Santamaría, J. M., and Zabalza, J.: Source origin of trace elements in PM from regional background, urban and industrial sites of Spain, *Atmos. Environ.*, 41, 7219–7231, 2007.
- Reche, C., Moreno, T., Amato, F., Viana, M., van Drooge, B. L., Chuang, H.-C., Bérubé, K., Jones, T., Alastuey, A., and Querol, X.: A multidisciplinary approach to characterise exposure risk and toxicological effects of PM₁₀ and PM_{2.5} samples in urban environments, *Ecotox. Environ. Safe.*, 78, 327–335, 2012.
- Richard, A., Bukowiecki, N., Lienemann, P., Furger, M., Fierz, M., Minguillón, M. C., Weideli, B., Figi, R., Flechsig, U., Appel, K., Prévôt, A. S. H., and Baltensperger, U.: Quantitative sampling and analysis of trace elements in atmospheric aerosols: impactor characterization and Synchrotron-XRF mass calibration, *Atmos. Meas. Tech.*, 3, 1473–1485, doi:10.5194/amt-3-1473-2010, 2010.
- Richard, A., Gianini, M. F. D., Mohr, C., Furger, M., Bukowiecki, N., Minguillón, M. C., Lienemann, P., Flechsig, U., Appel, K., DeCarlo, P. F., Heringa, M. F., Chirico, R., Baltensperger, U., and Prévôt, A. S. H.: Source apportionment of size and time resolved trace elements and organic aerosols from an urban courtyard site in Switzerland, *Atmos. Chem. Phys.*, 11, 8945–8963, doi:10.5194/acp-11-8945-2011, 2011.
- Salcedo, D., Laskin, A., Shutthanandan, V., and Jimenez, J. L.: Feasibility of the detection of trace elements in particulate matter using online high-resolution aerosol mass spectrometry, *Aerosol Sci. Tech.*, 46, 1187–1200, doi:10.1080/02786826.2012.701354, 2012.
- Theodosi, C., Grivas, G., Zarnpas, P., Chaloulakou, A., and Mihalopoulos, N.: Mass and chemical composition of size-segregated aerosols (PM₁, PM_{2.5}, PM₁₀) over Athens, Greece: local versus regional sources, *Atmos. Chem. Phys.*, 11, 11895–11911, doi:10.5194/acp-11-11895-2011, 2011.
- Turóczy, B., Hoffer, A., Tóth, Á., Kováts, N., Ács, A., Ferincz, Á., Kovács, A., and Gelencsér, A.: Comparative assessment of ecotoxicity of urban aerosol, *Atmos. Chem. Phys.*, 12, 7365–7370, doi:10.5194/acp-12-7365-2012, 2012.
- Viana, M., Kuhlbusch, T. A. J., Querol, X., Alastuey, A., Harrison, R. M., Hopke, P. K., Winiwarter, W., Vallius, A., Szidat, S., Prevot, A. S. H., Hueglin, C., Bloemen, H., Wahlin, P., Vecchi, R., Miranda, A. I., Kasper-Giebl, A., Maenhaut, W., and Hitzenberger, R.: Source apportionment of particulate matter in Europe: A review of methods and results, *J. Aerosol Sci.*, 39, 827–849, doi:10.1016/j.jaerosci.2008.05.007, 2008.
- Wedepohl, K.: The composition of the continental crust, *Geochim. Cosmochim. Ac.*, 59, 1217–1232, doi:10.1016/0016-7037(95)00038-2, 1995.
- Weijers, E. P., Schaap, M., Nguyen, L., Matthijsen, J., Denier van der Gon, H. A. C., ten Brink, H. M., and Hoogerbrugge, R.: Anthropogenic and natural constituents in particulate matter in the Netherlands, *Atmos. Chem. Phys.*, 11, 2281–2294, doi:10.5194/acp-11-2281-2011, 2011.
- Witt, M. L. I., Meheran, N., Mather, T. A., de Hoog, J. C. M., and Pyle, D. M.: Aerosol trace metals, particle morphology and total gaseous mercury in the atmosphere of Oxford, UK, *Atmos. Environ.*, 44, 1524–1538, doi:10.1016/j.atmosenv.2010.01.008, 2010.
- Wood, C. R., Lacer, A., Barlow, J. F., Padhra, A., Belcher, S. E., Nemitz, E., Helfter, C., Famulari, D., and Grimmond, C. S. B.: Turbulent flow at 190 m height above London during 2006–2008: A climatology and the applicability of similarity theory, *Bound.-Lay. Meteorol.*, 137, 77–96, doi:10.1007/s10546-010-9516-x, 2010.
- Xiao, Z. H., Shao, L. Y., Zhang, N., Wang, J., and Wang, J. Y.: Heavy metal compositions and bioreactivity of airborne PM₁₀ in a valley-shaped city in northwestern China, *Aerosol Air Qual. Res.*, 13, 1116–1125, doi:10.4209/aaqr.2012.10.0287, 2013.
- Zhou, J. A., Ito, K., Lall, R., Lippmann, M., and Thurston, G.: Time-series analysis of mortality effects of fine particulate matter components in Detroit and Seattle, *Environ. Health Persp.*, 119, 461–466, doi:10.1289/ehp.1002613, 2011.
- Zhou, Y. and Levy, J. I.: The impact of urban street canyons on population exposure to traffic-related primary pollutants, *Atmos. Environ.*, 42, 3087–3098, 2008.